



Propulsion System Integration and Hull Optimization for a Sailing-Cargo Vessel

submitted on 12th August 2020

by

RUIZ BUENDÍA Nicolás, Calle 134a#55a-46, 111111, nicsolas@gmail.com

Student ID No: S183806 (ULG)

Supervisor:

Paul Regnacq
Naval Architect
Bureau Mauric
44000 Nantes
France



This Master Thesis has been prepared as part of the graduation of the Master in Marine Technology specialized in Hydrodynamics for Ocean Engineering from Centrale Nantes and the graduation of the double Master degree Liège University-Centrale Nantes in the EMship+ programme

[This page intentionally left blank]

Abstract

The increase in regulations to reduce the carbon print from ship industry has become a motivating factor for the development of new and innovative types of propulsion systems. Also the validation of simulation tools with experimental test has become a decisive factor for the application of optimization strategies using simulations for the ship industry.

First the integration of the propulsion system for a sailing cargo vessel was carried out following the guidelines given by the supplier and based on these definition an adaptation to the previous form of the skeg from the concept design has been done based on the impact on additional terms of resistance and the performance in sailing condition.

An hydrodynamic optimization was performed using low fidelity solvers (*Shipflow*) and a successive validation with high-fidelity solvers (ISIS-CFD). Firstly, a multi-objective optimization with *Genetic Algorithms*, (*MOGA*) was carried out by using the Generalized Lackenby Semi- Parametric transformation for the fore-body of the hull, considering the wave resistance coefficient for the trial velocities as a objective functions using *Potential Flow Theory*.

Based on the results from the first phase of the optimization a single- objective optimization of the total resistance using the Zonal Approach to consider the viscous effects on the aft-body of the hull was performed. Considering the increase on computation time required when the viscous effects are considered using *RANS* equations. The optimization strategy was based on the definition of the design space by using sampling methods, Sensitivity Analysis. In order to reduce the design space to being able afterwards to use local objective optimization methods which are characterized for the fast convergence, requiring few evaluations of the objective function *T-Search Method*.

Significant reductions on the total resistance and powering required for the optimized hull were obtained, with a reduction around of 2.5%.

[This page intentionally left blank]

Acknowledgments

In first place, I want to thank God and the Colombian National Navy, which, through COTECMAR (Science and Technology Corporation for Naval, Maritime and Riverine Industry Development), supported me in one of the most enriching experiences in my life, both academically and personally. I will be thankful forever.

I would also like to express my gratitude to Mr. Vincent Seguin, CEO of Mauric Desing Novators, who trusted me to work in the company, my tutor Paul Regnacq and Jean Marc Deux. It was a pleasure to work under their supervision, being guided and supported with great care and cordiality. It really is an honour to have learned so much from your experience and knowledge Thanks for your lessons and unconditional support.

In third place, I want to thank all my professors and EMSHIP administrative staff for all their support and lessons. Specially, I want to thank professors Phillipe Rigo, Lionel Gentaz, Andre Hage and every other member of the Hydrodynamic Lab of the Ecole Centrale de Nantes (LHEEA). I definitely chose the best option at studying in this prestigious university. A very special thank you goes to all my colleagues from the M120, I admire you all.

In fourth place, I want to thank Dr. Stephan Harries, CEO of Friendship Systems enterprise, who permitted me the usage of the parametric optimization software CAESES and serving as a constant reference for the development of this work.

Last, but not least, I want to thank my family. My wife, my parents, and my brothers, who have been the engine behind all the strength and effort that I have put in every challenge of my life, specially while I developed this work. Thank you all so very much.

[This page intentionally left blank]

Contents

Abstract	iii
Acknowledgments	v
List of Figures	viii
List of Tables	ix
1 INTRODUCTION	1
1.1 AIMS AND OBJECTIVES	2
1.2 METHODS AND PROCEDURES	2
1.3 LITERATURE REVIEW	3
1.4 STRUCTURE	4
2 THEORY BACKGROUND	5
2.1 OPTIMIZATION	5
2.1.1 Sampling Methods	5
2.1.2 Local Optimization Methods	6
2.1.3 Global Optimization Methods	6
2.2 RESISTANCE AND PROPULSION	7
2.2.1 Resistance	7
2.2.2 Propulsion	10
2.3 POTENTIAL FLOW	12
2.3.1 Governing Equations and Hypothesis	13
2.3.2 Velocity Potential	13
2.3.3 Boundary Conditions	14
2.3.4 Linearization of the free surface boundary conditions	14
2.3.5 Radiation Condition	15
2.4 Viscous Flow - RANS	15
2.4.1 Governing Equations	15
2.4.2 Turbulence modeling	17
3 SHIP MAIN CHARACTERISTICS	22
3.1 Propulsion System	22
3.1.1 Hybrid Propulsion System	22
3.2 Skeg design	23
4 INITIAL CFD CALCULATIONS	25
4.1 SIMULATIONS SET-UP	25
4.1.1 Mesh generation	25

4.1.2	Flow settings	28
4.2	RESISTANCE AND POWERING	29
4.2.1	Case 1: No leeway	29
4.2.2	Case 2: Leeway Condition	32
4.2.3	Analysis and Results	36
5	HULL OPTIMIZATION	37
5.1	SHIPFLOW STRUCTURE	37
5.2	PARAMETRIC MODELLING OF THE HULL	38
5.2.1	Semi - Parametric approach	38
5.2.2	Fully- parametric approach	39
5.3	FORWARD OPTIMIZATION - POTENTIAL FLOW	41
5.3.1	Mesh Convergence Study	41
5.3.2	Multi- Objective Optimization	43
5.4	SKEG OPTIMIZATION - ZONAL APPROACH	48
5.4.1	Mesh discretization	48
5.4.2	Single Objective Optimization	49
6	Conclusion and Recommendations	54
	References	55

List of Figures

1	Hydrodynamic performance optimization based on CFD [6]	2
2	Double body flow [7]	8
3	Secondary wave system [7]	9
4	Resistance decomposition [7]	9
5	Reynold's decomposition [12]	16
6	Boundary Layer profiles [4]	20
7	Initial hulls concept design	23
8	U and V skeg forms	24
9	Domain of the simulation	26
10	Mesh Version 1	27
11	Mesh Details Version 2	28
12	Absolute error Resistance Case No 1.	30
13	Wake Flow 14 Kn	31
14	Power- Speed estimation	32
15	Resistance curve Condition No 2	33
16	Difference Sway Forces $\lambda = 5^\circ$	34
17	Sway Forces by Section	35
18	Anti-drift fins [2]	35
19	Zonal- Approach <i>Shipflow</i>	37
20	Fully- parametric skeg	40
21	Zonal- Approach <i>Control points</i>	40
22	Skeg transformations Fully -parametric approach	41
23	Fully- parametric skeg	42
24	Comparison coarse and medium mesh	43
25	Classic Lackenby and Generalized Lackenby method [5].	44
26	Generalized Lackenby representation	45
27	Convergence history plot objective functions	46
28	MOGA Comparison	46
29	Sectional Area Curve plot	47
30	Comparison of the wave profiles of parent and optimized design	47
31	Wave Contour and Pressure coefficient comparison for 13 Kn	48
32	Viscous domain	49
33	Boundary conditions Zonal Approach	49
34	Sensitivity Analysis design Variables	51
35	Convergence History Objective Function	53

List of Tables

1	SST $k - \omega$ model coefficients	19
2	Distance constraints	24
3	Number of cells different meshes	27
4	Efficiencies propulsion system	31
5	Discretization of meshes	43
6	Hydrostatic Properties Variation Fore-body Optimization	46
7	Design variables "Sensitivity Analysis"	50
8	Design variables "T- Search Method"	52
9	Resistance and Powering comparison optimized hull for 14 Kn	53

[This page intentionally left blank]

DECLARATION OF AUTHORSHIP

I declare that this thesis and the work presented in it are my own and have been generated by me as the result of my own original research.

Where I have consulted the published work of others, this is always clearly attributed.

Where I have quoted from the work of others, the source is always given. With the exception of such quotations, this thesis is entirely my own work.

I have acknowledged all main sources of help.

Where the thesis is based on work done by myself jointly with others, I have made clear exactly what was done by others and what I have contributed myself.

This thesis contains no material that has been submitted previously, in whole or in part, for the award of any other academic degree or diploma.

I cede copyright of the thesis in favour of the Ecole Centrale de Nantes and Mauric.

Date: 12/08/2020

Signature:

[This page intentionally left blank]

1 INTRODUCTION

Nowadays, several regulations are being created in order to reduce emissions and contamination from the ship industry and, as a consequence, the need to produce energy efficient ships has increased substantially. For instance the IMO (International Maritime Organization) controls NO_x (Nitrogen Oxide) emissions from Diesel Engines worldwide, based on the areas of navigation, construction year, and type of ship [20]. Based on the aforementioned claims, this master thesis is focused on the selection of a propulsion system and the hydrodynamic optimization of a sailing cargo vessel, which was created in order to develop new ship designs, aiming at meeting IMO emissions regulations' standards. The proposal consists on a new hybrid propulsion system that combines diesel and electric engines, while using sails to acquire an important amount of additional power from wind. This proposal both complies with the regulations and provides effective solutions to the transportation field.

Several ways to measure ship's resistance and power exist nowadays, such as empirical methods based on statistical approaches from parent designs, *EFD* (Experimental Fluids Dynamics) and *CFD* (Computational Fluid Dynamics) [7]. Currently, due to high fidelity achieved through *CFD* validations, most designs are carried out using this method from the earliest to the latest phases. During such latest phases, results are validated with *CFD*, achieving good resemblance between numerical and experimental results, but also opening the possibility to test multiple designs, thereby reducing time and money costs spent on experimental tests.

Designing a ship is a complex process, which starts with the owner's demands, and ends with the operation of the ship. This process involves different design stages; the concept, preliminary, detailed and production design [6]. *SDD* (Simulation Driven Design) moves simulation technology to the earliest stages of the design process, therefore, considerably reducing time and resources spent by a company on design, using the simulation technology to create the design and not to validate it, as has been done in the past [21].

The main goal on ship design is to satisfy all the requirements of the client on a technical manner, optimizing resources and improving performance. Different goals can be pursued on ship design optimization, such as the reduction of structure weight, and, consequently, the displacement of the ship. Also the hydrodynamic optimization; reducing resistance and powering or the sea-keeping characteristics of the ship. This project is based on the ship hull optimization, to reduce resistance and powering of the ship. This is a highly complex process requiring the integration of *CFD*, *CAD* (Computer Aided Design), optimization methods and *Grid* technologies.

1.1 AIMS AND OBJECTIVES

Different objectives are derived from the main aim of project *NEOLINER* which is the design of environmentally friendly energy solutions for the ship cargo industry, one of the main sources of worldwide pollution [6]. In order to achieve this goal the following objectives are defined:

- Definition of the propulsion system.
- Design and comparison of different skeg forms following the guidelines provided by the propulsion systems suppliers, which is focused on better hydrodynamic performance: resistance prediction, and course stability.
- Hydrodynamic optimization of the aft and fore-body of the hull based on *CFD* for the main operation velocities on calm water conditions.

1.2 METHODS AND PROCEDURES

CAESES is a Computer-aided engineering environment *CAE* software developed by Friendship Systems which is a spin-off company from the *Technical University of Berlin*. CAESES combines process integration and design optimization with a flexible automated parametric geometry variation, and integrates with a variety of *CFD* simulation software. It is one of the most widely used software for *SDD* on the marine industry.

In **Fig. 1** an overview of the optimization process based on *CFD* simulations is displayed.

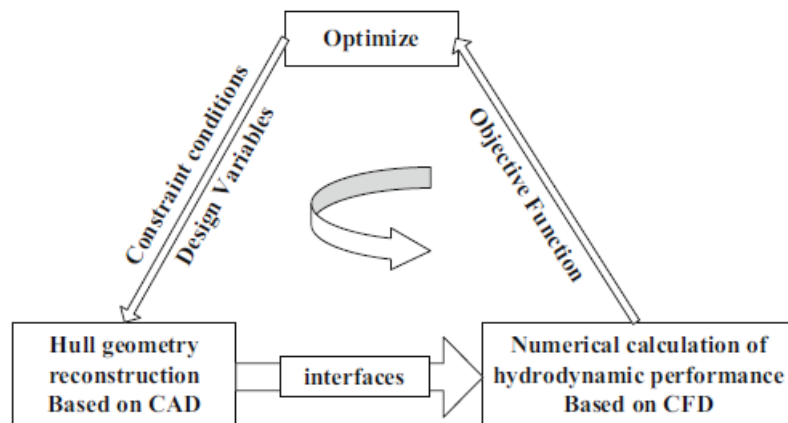


Figure 1: Hydrodynamic performance optimization based on CFD [6]

The procedure of *SDD* optimization is divided into five different components [21]:

- Geometry variation: A parametric model of the ship is defined and the transformed geometry is created.

- Pre-processing: All the design variables are pre-processed in order to define if the model is a feasible design to continue with the simulation. On this part the design constraints are considered.
- Simulation: The simulation of all feasible designs is carried out.
- Post-processing: The results from the simulation are processed and visualized.
- Optimization: Based on the selected optimization strategy different variants of the geometry are performed repeating this sequence until an optimum design is obtained.

1.3 LITERATURE REVIEW

An extensively studied field of ship hydrodynamics is the determination of the total resistance of a ship moving with a constant speed on calm water. Hence, the optimization of the total resistance of the ships has been a pressing topic by several researchers since the 19th century [13].

Early developments on ship design optimization until 1990s were based on the reduction of the wave resistance using the *Michell* integral method [19], optimizing the fore-body of the ship. However, due to the simplified assumptions on the surface and free surface conditions by linear theory, the “peak” and “valley” values of wave resistance are excessively exaggerated. A compilation on the literature on geometric hull modelling and CFD based hull optimization was done by Harries [22].

After 1990s, researchers began to use the *Rankine source method* of the potential flow theory for hull optimization, resulting better agreement between the results obtained during the optimization and the validation of the designs with EFD [6]. Some of the most representative developments were done by Harries [22][5], Campana [11] and Susuki [17].

Due to the rapid development of CFD, the computational power, storage capacity, and optimization strategies, the SDD based on RANS (Reynolds Averaged Navier Stokes Equations) equations has become a new research direction for ship hull optimization in which viscous effects are now considered as well.

Literature related to hull modeling and CFD based hull optimization from different researchers and industrial companies has been considered during this work.

A general idea of the optimization methods for ship hydrodynamic design were taken from Campana et al [11] where single and multi-objective optimization problems are considered. The description of different optimization methods such as derivative and non derivative methods is presented in detail and the different strategies based on the complexity of the problem are given.

1.4 STRUCTURE

In this chapter the structure of the report is explained. Chapter 1 gives a general introduction of the work with motivation, objectives, and a literature review.

In Chapter 2 a brief description of the optimization algorithms used during the optimization is provided. A theoretical background about resistance and propulsion estimation is given with a description of the methods used to perform the simulations.

Chapter 3 describes the main characteristics of the ship, with the definition of the propulsion system. Based on this definition four different types of hulls were defined.

In Chapter 4, several simulations are performed and analyzed for two conditions; resistance on calm sea, and resistance and lateral forces for a leeway condition to the different hull forms proposed in the previous chapter. The comparison of the results are done and the best hull form with superior performance is selected.

Chapter 5 is the core of this work in which the optimization of the hull is carried out. The aft and fore-body of the hull is optimized using low-fidelity solvers. At the end, a validation of the results is briefly discussed using high-fidelity solvers.

2 THEORY BACKGROUND

2.1 OPTIMIZATION

Ship hull form optimization is a highly complex non-linear problem in which different design variables and constraints are involved. Due to its complexity, different optimization techniques are proposed to find the global optimum solution for ship hull optimization. Single and multi-objective optimization approaches can be used on ship hull optimization. However, a single objective optimization routine normally improves the design for the objective function but also reduces the performance of the hull for other conditions [11]. Due to this fact, hull optimization is widely used using multiple-objective optimization methods.

During the course of this work, local and global optimization algorithms integrated in the CAESES environment were used to find the optimum solution. In order to reduce the computation time of the optimization problem, the two approaches can be combined to take the advantages of both of them, which is widely used on ship hull hydrodynamics, this is called a hybrid optimization approach [6].

A typical engineering hull optimization problem as mentioned before involves different design variables and constraints and can be defined as follows.

$$\begin{aligned}
 & \text{minimize} && f(\mathbf{X}) \\
 & \text{subject to} && g_i(x) = 0 \\
 & && h_j(x) \leq 0
 \end{aligned} \tag{1}$$

where $g(x)$ and $h(x)$ are the equality and inequality constraints, \mathbf{X} is the vector of design variables and f is the objective function to be minimized.

2.1.1 Sampling Methods

Sensitivity Analysis

Sensitivity Analysis is a useful technique to identify the influence of the design variables on the objective function. Sensitivity Analysis is performed prior to the optimization routine to identify which design variable has a stronger influence on the response, and also to limit their bounds.

This sampling technique developed by *Dakota* and integrated in the CAESES environment is able to generate sets of samples according to probability distributions and a number of samples defined by the user. This method uses the *LHS* (Latin Hypercube Sampling) in which the range of each variable is divided into N_S segments of equal probability. Where

N_S is the number of samples requested providing a uniform distribution of all the design space.

2.1.2 Local Optimization Methods

Local optimization methods have the ability to quickly converge to the local minimum closest to the starting point. As a consequence, a high dependence on the starting point is a major drawback of these type of methods.

Tangent Search Method

The Tangent search of constrained minimization method proposed by Hilleary [14] is an adaptation of the *Direct Search method* well suited for small scale single objective optimization problems, in which inequality constraints are involved. One of the advantages of this method is the detection of a descent search direction of the solution space with fast convergence to the optimum. However, this method is sensible to the starting point and the step size of the exploratory moves.

An exploratory move involves the process taken to find the the optimum based on perturbations of the starting point to find the descent direction. Due to this fact, the starting point of this method and the bounds of the design variables are taken from previous analysis based on sampling methods.

2.1.3 Global Optimization Methods

Considering the drawbacks and limitations of the local based optimization methods, the unavailability of the derivatives and difficulties to find a descent direction. Currently, ship hull hydrodynamics aims to shift from local to global non derivative optimization methods. The goal of this method is to ensure the effectiveness and efficiency in terms of number of objective functions evaluated. However, with these methods there is no proof of convergence to the global optimum.

Multi- Objective Optimization

Under multi-objective optimization problems, the concept of global solution is no longer available. For the selection of the best design, different minimum points can be found considering the different objective functions. In order to define the optimal design for these type of problems, the optimum trade-off proposed by Pareto is used [11]. The trade-off entails the concept of domination by dividing the solution into two different sets, the dominated and non-dominated solutions. The optimal solutions are defined as the points located on the boundary in which no improvement of the solution can be obtained and it is called the dominating design. The dominated designs are those solutions which can be im-

proved by another design, the location of the dominated points is outside of the Pareto front.

Multi-Objective Genetic Algorithm MOGA

The genetic algorithms (*GA*) are based on biological evolution which simulates the Darwin's natural evolution law of the "natural selection and survival of the fittest"[6]. The search of the optima is not dependent on the gradient information of the problem being used for complex non linear problems, such as hull optimization. This algorithm has five steps:

- Initialization: Initial population of individuals based on a random manner.
- Fitness evaluation: Evaluation of each individual based on quality criterion.
- Selection of individuals: Selection based on a probability proportional to their fitness.
- Crossover: Combine two individuals to create new individuals for inclusion in the next generation.
- Mutation: Slight modification of the resulting new individuals in order to maintain the diversity of the new generation.

The process from the fitness evaluation to the mutation is repeated until the maximum number of generations is achieved. The convergence of this method is slow and requires many evaluations of the objective function. Due to this fact, it is used in problems where the evaluation of the objective function is not expensive in terms of computation power.

2.2 RESISTANCE AND PROPULSION

The correct estimation of the resistance is an important part during the design process of a ship in order to define correctly the required power to move the ship at the required velocities. Also, the correct estimation enables the designer to select the propulsion system having a good idea of the power required by the engine. Thereby, enabling the efficient definition of the sizes and masses of the propulsion system, and also determining the operational costs of the ship for a given operation profile.

2.2.1 Resistance

Decomposition of the resistance

The total resistance of a ship is the sum of the contributions of different resistance terms. The total resistance comes from the model tests on calm waters and validation of tests due to the impossibility of measuring the resistance at full scale.

The total resistance can be decomposed in the following terms [7]:

- *Friction resistance:*

The friction resistance is mainly due to the effect of the viscosity, and states that the

fluid particle is attached to the hull hence at the same velocity of the hull. However, at some distances away from the hull there is a variation in the velocity of the particle reaching after the velocity of the inviscid flow. This region between the hull surface and the flow is known as the boundary layer. This variation of the velocity on the normal direction in the boundary layer induces shear stresses yielding to the friction resistance which is also function of the wetted surface area.

- *Viscous Pressure resistance:*

Due to the different hull forms of ships, a local flow is induced with velocity variations higher or lower than average velocity. Then, the shear stress inducts additional viscous resistance, this resistance is less in slender ships compared with full ship forms.

- *Wave resistance:*

The waves produced by the ship contribute to the total resistance, this wave resistance can be decomposed into two wave systems.

Primary wave system

From the *D' Alembert's* paradox a deeply submerged body in a fluid with no viscosity has zero resistance. A variation of the velocity in the flow consequently create a variation on the pressure. For ship applications, the submerged body of the ship below the calm water surface is mirrored. This double body creates a pressure distribution at the symmetry plane in an infinite ideal fluid. A corresponding surface elevation is a consequence of this pressure distribution under *Bernoulli's* equation yielding to wave crests at the end of the ship and trough in the middle. This primary wave system is independent of the speed [7].

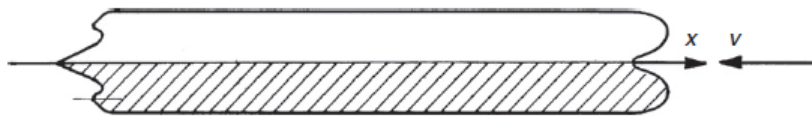


Figure 2: Double body flow [7]

Secondary wave system

The waves produced by the geometry and the speed of the ship induce an additional resistance that must be considered in the total resistance. These waves are formed by the interaction of the produced waves, where strong changes in the geometry near the water surface occur, such as the bow, shoulders and stern. The interaction between them result in the additional wave resistance named as secondary wave system composed by divergent and transverse waves.

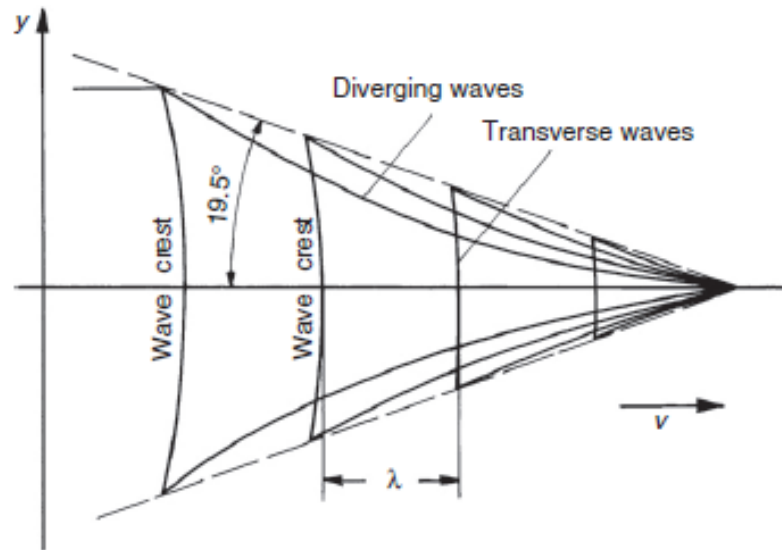


Figure 3: Secondary wave system [7]

Fig. 4 shows the decomposition of the total resistance.

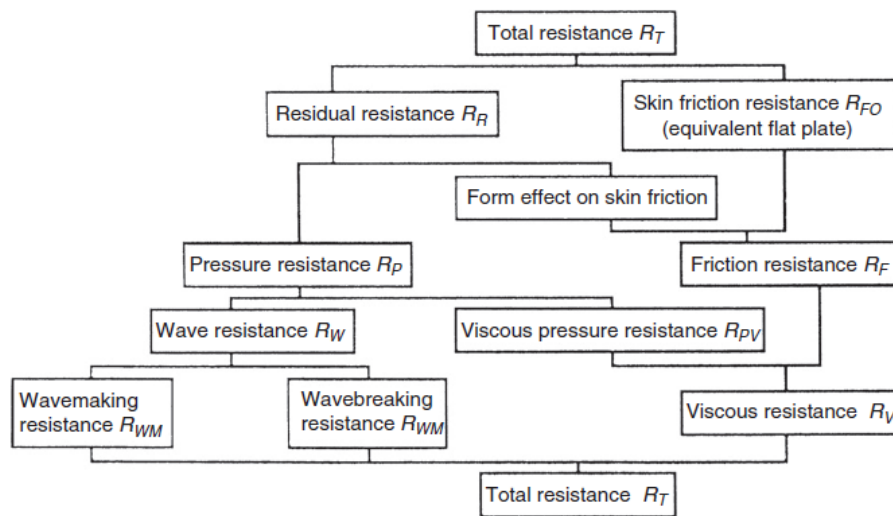


Figure 4: Resistance decomposition [7]

Calculation approaches

Different methods are used in order to get a good estimation of the resistance. In the past, some statistical methods have been proposed based on series of experiments from parent hull forms making it possible to determine the required coefficients from those series of ships. Nowadays, due to the elevated cost and the time required to make these experiments, the constant development of numerical methods and increase in computational power, there are no recent comparable series of modern hulls tested [7].

The experimental approaches in model tests or full scale trials are widely used for validation

of the results from several computations using numerical methods. In this work, *CFD* are used due to the ability of testing different hulls and predicting resistance and powering with a good level of confidence. These methods are explained on detail in **Sections 2.3** and **2.4**.

2.2.2 Propulsion

The hull-propeller interaction has a strong influence on the power prediction. In the past, this relation has been studied independently introducing some special efficiencies and factors to consider the interaction between the propeller and the hull. Analyzing the hull under resistance tests (numerical or experimental), and the propeller in open waters with the same methods. However, recent progress in ship hydrodynamics is making it possible to integrate this interaction and, as a result, it is now possible to estimate the powering based on self propulsion studies in numerical and experimental approach using actual propulsion.

Power definition

The power is obtained from the product between a force and a given speed. In naval hydrodynamics the effective power P_E is the result between the total resistance of the hull in calm water R_T as explained in **Section 2.2.1** and the velocity of the ship V_s .

$$P_E = R_T \times V_s \quad (2)$$

Being the power required to tow the ship without the presence of a propulsion system, once the propulsion system is considered with the hull-propeller interaction, a new expression called the thrust power P_T is obtained.

$$P_T = T \times V_A \quad (3)$$

Where V_A is the speed of advance and T is the thrust measured from propulsion tests. The thrust is higher than the total resistance as a consequence of induced resistance by the propeller, due to the effect on the frictional resistance by the increased flow velocity in the aft-body by the propeller and decrease in pressure of the aft-body, thus increasing the inviscid resistance. An additional factor links the thrust and the resistance, this factor is called the thrust deduction factor t .

$$t = 1 - \frac{R_T}{T} \quad (4)$$

Wake Factor

Due to the action of the wake which is influenced by the hull forms, the speed of advance

previously mentioned on **Eq. 3** is the result of a reduction in the speed of the flow at the propeller, comparing it with the ship velocity. This wake is decomposed into three different components: *Friction wake*, *Potential wake* and *Wave wake*, for single screw ships the friction wake is dominant [7].

- *Friction wake:*

The viscosity effects leads to flow separation in regions of high curvatures, thus, the velocity is reduced in the boundary layer compared to the ship velocity.

- *Potential wake:*

At the stagnation point it is predictable to have low velocities. In an ideal fluid without viscosity the flow velocity at the stern is the same at the bow.

- *Wave wake:*

As mentioned in **Section 2.2.1** the wave system also affects the flow and as a consequence an increased flow velocity is expected when a wave crest is above the propeller and lower when it is a trough.

The wake fraction w can be calculated with **Eq. 5**.

$$w = 1 - \frac{V_A}{V_S} \quad (5)$$

Propulsive Efficiencies and Powering

Several losses of energy are considered throughout the propulsion system, and different definitions of powers and efficiencies have to be taken into account. Based on the definitions for the wake fraction w and thrust deduction factor t from **Eqs. 4 and 5** the hull efficiency η_H can be obtained.

$$\eta_H = \frac{P_E}{P_T} = \frac{R_T \cdot V_S}{T \cdot V_A} = \frac{1 - t}{1 - w} \quad (6)$$

An additional efficiency term known as propeller efficiency behind the ship is considered η_B being able to define the delivered power P_D which is higher than the previous thrust power P_T . This efficiency behind the ship is calculated based on the efficiency of the propeller in open water η_0 , and the relative rotative efficiency η_R considering the differences between the flow seen by the propeller in open water tests and the actual flow encountered in propulsion conditions.

$$P_D = 2\pi \cdot n \cdot Q \quad (7)$$

Additional efficiencies are taken into account due to the losses from the shaft and the gearbox. These efficiencies can be expressed in a simple form as shaft efficiency η_S , normally the value for this efficiency is around 0.98%-0.99%, and, as a consequence, the power delivered by the engine P_B is defined.

$$P_B = \frac{P_D}{\eta_S} \quad (8)$$

Then the effective power P_E defined on **Eq. 2** can be expressed in terms of the efficiencies involved in the propulsion system as follows.

$$P_E = \eta_D \cdot \eta_S \cdot P_B \quad (9)$$

Where η_D is the propulsive efficiency considering the hydrodynamic efficiencies $\eta_H \cdot \eta_0 \cdot \eta_R$.

Sailing Vessels Resistance

Additional terms for resistance are considered for a sailing vessel, having an induced drag produced by the keel, fins and rudders when the ship has some leeway angle. This lift produced by the appendages is important to resist the side forces produced by the sails and to ensure the course stability. The resistance of a sailing vessel can be expressed with the following equation [1]:

$$R_T = R_{Fh} + R_{Rh} + R_{VK} + R_{VR} + R_{RK} + \Delta R_{Rh} + \Delta R_{RK} + R_{Ind} \quad (10)$$

Where:

- R_T is the total resistance of the ship considering the appendages at a heel and leeway angle.
- R_{Fh} is the frictional resistance of the hull.
- R_{Rh} is the residuary resistance of the hull.
- R_{VK} is the viscous resistance of the keel.
- R_{VR} is the viscous resistance of the rudder.
- R_{RK} is the residuary resistance of the keel.
- ΔR_{Rh} is the change in residuary resistance of the hull with the heel angle ϕ .
- ΔR_{RK} is the change in residuary resistance of the keel with the heel angle ϕ .
- R_{Ind} is the induced resistance due to the side force generation and the leeway angle λ .

2.3 POTENTIAL FLOW

In order to solve the steady ship wave system, the Nonlinear free surface rankine method is used.

Boundary Value Problem

The boundary value problem can be analyzed by boundary integral equations. By using the BEM (Boundary Element Method), an approximate numerical solution of the boundary integral equations is obtained. In order to solve this value problem, a discretization of the

boundary conditions has to be done. In this case study, the hull and the free surface with linear or higher order panels. The pressure forces and velocities are evaluated from the linearized system of equations with the distribution of the singularities along the panels, enforcing the boundary conditions on each panel.

2.3.1 Governing Equations and Hypothesis

Under the assumption that the ship advance with a constant velocity $|\vec{U}_\infty|$, inviscid- ideal, incompressible fluid with irrotational flow. The flow is described in an Eulerian sense in which the reference coordinate is fixed to the ship with the same speed, but not following its dynamic trim and sinkage [16].

Under these assumptions, the governing equation of the flow is the continuity equation:

$$\frac{\partial \rho}{\partial t} + \frac{\partial(\rho u)}{\partial x} + \frac{\partial(\rho v)}{\partial y} + \frac{\partial(\rho w)}{\partial z} = 0 \quad (11)$$

Considering that the pressure is not dependant of time the derivative is removed and from **Eq 11** equation the following is obtained.

$$\frac{\partial(u)}{\partial x} + \frac{\partial(v)}{\partial y} + \frac{\partial(w)}{\partial z} = 0 \quad (12)$$

From the assumption of irrotational flow then the velocity can be defined as a potential of the flow:

$$rot \vec{V} = \vec{0} \Rightarrow \exists \phi \quad (13)$$

As a consequence, the velocity vector is expressed as the gradient of the velocity potential ϕ and it can be expressed according the following equation:

$$\vec{V} = \nabla \phi \quad (14)$$

Introducing equation **Eq 14** into **Eq 12** the Laplace equation is obtained.

$$\nabla^2 \phi = 0 \quad (15)$$

2.3.2 Velocity Potential

With the same assumptions as previously stated, the velocity components can be determined as a gradient of a scalar function ϕ composed by the potential of undisturbed flow ϕ_∞ and the potential of the disturbed flow caused by the ship ϕ' . Utilizing the principle of superposition the total potential can be obtained from the two potentials mentioned before.

$$\phi = \phi_\infty + \phi' \quad (16)$$

2.3.3 Boundary Conditions

The potential flow is solved in an iterating manner of distribution of singularities along the panels.

Kinematic and Dynamic hull boundary conditions

The boundary condition is defined to the hull surface in which the velocity potential should be a known component equal to zero in the normal direction due to the impossibility of any particle to pass through a rigid body.

$$\frac{\partial\phi}{\partial n} = 0 \quad (17)$$

Kinematic and Dynamic free surface boundary conditions

Two more boundary conditions are imposed with the presence of free surface and they have to be fulfilled at the unknown position of the free surface.

The first condition is the kinematic free surface condition implying that the flow is tangential to the free surface and as a consequence, no particle is able to leave the surface. Thus, the flow potential in the normal direction of the free surface is equal to zero:

$$\frac{\partial\phi\partial\eta}{\partial x\partial x} + \frac{\partial\phi\partial\eta}{\partial y\partial y} - \frac{\partial\phi}{\partial z} = 0 \quad (18)$$

With η being the normalized distance from the free surface to the initial undisturbed free surface.

The dynamic free surface boundary condition proceeds from the **Bernoulli's** equation which states that the pressure on the free surface must be constant and equal to the atmospheric pressure.

$$\eta + \frac{1}{2} \left[\left(\frac{\partial\phi}{\partial x} \right)^2 + \left(\frac{\partial\phi}{\partial y} \right)^2 + \left(\frac{\partial\phi}{\partial z} \right)^2 - 1 \right] = 0 \quad (19)$$

2.3.4 Linearization of the free surface boundary conditions

A linearization of the free surface boundary conditions has to be done considering that the **Equation 19 and 18** are non-linear and they have to be imposed in the unknown free surface. Different methods to linearize the free surface boundary conditions are proposed by different authors in a first order Taylor series expansion, introducing perturbations from the waves and the hull to the known solution. Higher order perturbations can be assumed as small and neglected.

Linearization proposed by Dawson is widely used by the Rankine panel solvers. This linearization is done around the double model body flow as base solution in which the surface is treated as a symmetry plane mirroring the underwater part of the hull and the

problem is solved in an iterative manner.

2.3.5 Radiation Condition

An additional condition has to be imposed to have a single mathematical solution implying that the disturbance velocity caused by the hull vanishes at infinity when a distance from the hull tends to infinity.

$$\lim_{r \rightarrow \infty} |\vec{\nabla} \phi'| = 0 \quad (20)$$

2.4 Viscous Flow - RANS

For complex flows governed by the turbulence effects with high Reynold's numbers and unsteady flow with large fluctuations in space and time like in Naval Hydrodynamics, the turbulence is governed by Navier Stokes equations. Different methods are proposed to capture this phenomenon characterized by the formation of eddies at different scales with transfer of energy between them from the bigger to the smallest. This phenomena can be calculated by DNS (Direct Numerical Simulation), LES (Large Eddy Simulation), where the *Kolmogrov scale* is modelled and with RANS where the turbulence at all scales is modelled. The first two methods requiring extremely dense grids to capture all the scales making not possible to use them at real scale for ship hydrodynamics, due to the existing limitations on computational power. As a consequence, nowadays the RANS using Reynold's decomposition models are widely used.

2.4.1 Governing Equations

From the continuity equation where the mass is conserved and under the assumption that only incompressible flow is considered **Eq. 21** can be written neglecting the influence of the density as **Eq.22**

$$\frac{1}{\rho} \frac{\partial \rho}{\partial t} + \frac{\partial U_i}{\partial x_i} = 0 \quad (21)$$

$$\frac{\partial U_i}{\partial x_i} = 0 \quad (22)$$

Then the motion Navier Stokes equations is written in the following form:

$$\rho \frac{\partial U_i}{\partial t} + \rho \frac{\partial (U_j U_i)}{\partial w_j} = \rho R_i + \frac{\partial \sigma_{ij}}{\partial x_j} \quad (23)$$

Where σ_{ij} is the total stress for a *Newtonian Fluid*.

$$\sigma_{ij} = -P \delta_{ij} + 2\mu \left(S_{ij} - \frac{1}{3} S_{kk} \delta_{ij} \right) \quad (24)$$

being the strain rate S_{ij} defined in the following form

$$S_{ij} = \frac{1}{2} \left(\frac{\partial U_i}{\partial x_j} + \frac{\partial U_j}{\partial x_i} \right) \quad (25)$$

for incompressible flow S_{kk} in **Eq. 24** is zero.

$$S_{kk} = \frac{1}{2} \left(\frac{\partial U_k}{\partial x_k} + \frac{\partial U_k}{\partial x_k} \right) = \frac{\partial U_k}{\partial x_k} = 0 \quad (26)$$

using the Reynold's decomposition, dividing the instantaneous velocity U_i and pressure P into a mean and fluctuating component \bar{U} , \bar{P} , u'' , p'' .

$$U = \bar{U} + u'' \equiv u + u'' \quad (27)$$

$$P = \bar{P} + p'' \equiv p + p'' \quad (28)$$

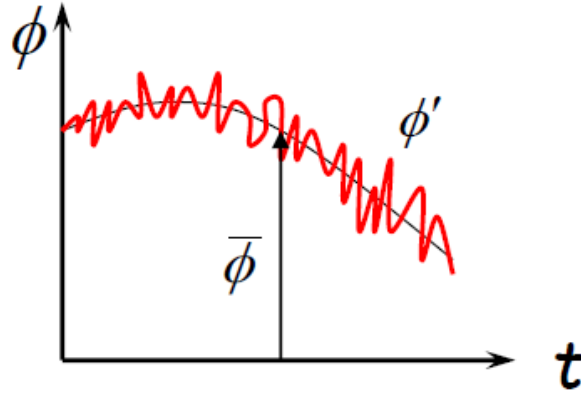


Figure 5: Reynold's decomposition [12]

The time mean of a variable is defined as

$$\bar{\phi} = \lim_{T \rightarrow \infty} \frac{1}{2T} \int_{-T}^T \phi dt \quad (29)$$

Using the average properties, with the time average the continuity equation gives

$$\frac{\partial \bar{U}_i}{\partial x_i} = \frac{\partial \bar{U}_i}{\partial x_i} = \frac{\partial u_i}{\partial x_i} = 0 \quad (30)$$

Subtracting **Eq. 30** from **Eq. 22** gives that the fluctuating velocity also follows the continuity equation

$$\frac{\partial u_i''}{\partial x_i} = 0 \quad (31)$$

The time average of Navier Stokes equation gives:

$$\begin{aligned}
& \overline{\rho \frac{\partial U_i}{\partial t} + \rho \frac{\partial (U_j U_i)}{\partial x_j} - \rho R_i + \frac{\partial P}{\partial x_i} - \frac{\partial}{\partial x_j} \left(\mu \left(\frac{\partial U_i}{\partial x_j} + \frac{\partial U_j}{\partial x_i} \right) \right)} = \\
& \rho \frac{\partial \bar{U}_i}{\partial t} + \rho \frac{\partial (\bar{U}_j \bar{U}_i)}{\partial x_j} - \rho \bar{R}_i + \frac{\partial \bar{P}}{\partial x_i} - \frac{\partial}{\partial x_j} \left(\mu \left(\frac{\partial \bar{U}_i}{\partial x_j} + \frac{\partial \bar{U}_j}{\partial x_i} \right) \right) = \\
& \rho \frac{\partial u_i}{\partial t} + \rho \frac{\partial (u_j u_i + \overline{u_j'' u_i''})}{\partial x_j} - \rho \bar{R}_i + \frac{\partial p}{\partial x_i} - \frac{\partial}{\partial x_j} \left(\mu \left(\frac{\partial u_i}{\partial x_j} + \frac{\partial u_j}{\partial x_i} \right) \right)
\end{aligned} \tag{32}$$

Then the time averaged continuity Navies Stokes equation is written in the following form under the assumption of incompressible flow

$$\begin{aligned}
& \frac{\partial u_i}{\partial t} + \frac{\partial (u_j u_i + \overline{u_j'' u_i''})}{\partial x_j} = \bar{R}_i - \frac{1}{\rho} \frac{\partial p}{\partial x_i} + \frac{\partial}{\partial x_j} \left(\nu \left(\frac{\partial u_i}{\partial x_j} + \frac{\partial u_j}{\partial x_i} \right) \right) \\
& \frac{\partial u_i}{\partial x_i} = 0
\end{aligned} \tag{33}$$

where ν is the kinematic viscosity

$$\nu = \frac{\mu}{\rho} \tag{34}$$

2.4.2 Turbulence modeling

A consequence of the time averaging of *Navier Stokes Equations* is the existence of six additional unknowns coming from the created tensor. Thus, requiring additional systems of equations in terms of known averaged quantities, this is known as the closure problem [3] and [4].

The new system of equations are taken by multiplying the *Navier Stokes equations* by a fluctuating property and time averaging the product, resulting on differential equations for the stress product, requiring turbulence models to solve these equations. The commonly used models are based on the *Boussinesq hypothesis* defining a simple relationship between Reynold's stresses and velocity gradients, through the *eddy viscosity*.

$$\rho \overline{u_i'' u_i''} = -\mu_T \left(\frac{\partial u_i}{\partial x_j} + \frac{\partial u_j}{\partial x_i} \right) + \frac{2}{3} \rho k \delta_{ij} \tag{35}$$

Different Eddy- viscosity turbulent models exist and they are classified based on the number of transport equations to be solved in addition to RANS equations. Simple models have been proposed to define the viscosity through velocity and length scales. Some of them solved by analytical approach (0 equation model), where V and L are given. One equation model where L is given and V is solved requiring one transport equation and

two equations models where V and L are solved requiring two transport equations. Two-equations models are widely used in Naval Hydrodynamics such as k -epsilon and k -omega models, in which one equation solves the turbulent kinetic energy, k and one additional equation the dissipation rate (ϵ, ω). These methods are tested and validated providing reliable results. However, the most used is the $k - \omega$ SST model proposed by Menter [18], which is used in the present work.

k - ω SST Model

Based on the existing two equations models $k - \omega$ and $k - \epsilon$, this model combines the advantages of both of them, using the zonal approach with $k - \omega$ model near the solid walls and $k - \epsilon$ is used outside this region. This switching is achieved with a blending function of the model coefficients. The $k - \omega$ model provides more realistic solutions for the flows in the boundary layer, previously overestimated by the $k - \epsilon$ models under adverse pressure gradient. This model is based on the Bradshaw's assumption in which the principal stress is proportional to the turbulent kinetic energy. It is also not sensible to the free stream ω value.

The $k - \epsilon$ model is transformed into $k - \omega$ formulations, the difference between this model and the original $k - \omega$ model is an additional cross-diffusion term appearing in the ω equation. In addition to different values for the constants of the model, $k - \omega$ model is multiplied by a function F_1 and $k - \epsilon$ by $1 - F_1$ adding the equation of both models together. This function F_1 has a value of one in the inner half part of the boundary layer and, afterwards, it vanishes, obtaining the baseline $k - \omega$ model.

In order to improve the prediction of separated flows and to avoid overestimated Reynolds stresses by the $k - \omega$ and $k - \epsilon$ models in adverse pressure gradients. An additional blending function F_2 is used in this model for the formulation of the eddy viscosity improving significantly the previous models.

The transport equations of the model are defined as follows.

$$\frac{\partial k}{\partial t} + \frac{\partial(u_j k)}{\partial x_j} = -\overline{u_i'' u_j''} \frac{\partial u_i}{\partial x_j} - \beta * k\omega + \frac{\partial}{\partial x_j} \left((v + \sigma_k v_T) \frac{\partial k}{\partial x_j} \right) \quad (36)$$

$$\frac{\partial \omega}{\partial t} + \frac{\partial(u_j \omega)}{\partial x_j} = -\frac{\gamma}{v_T} \overline{u_i'' u_j''} \frac{\partial u_i}{\partial x_j} - \beta * \omega^2 + \frac{\partial}{\partial x_j} \left((v + \sigma_\omega v_T) \frac{\partial \omega}{\partial x_j} \right) + 2\sigma_{\omega 2} \frac{1 - F_1}{\omega} \frac{\partial k}{\partial x_j} \frac{\partial \omega}{\partial x_j} \quad (37)$$

Where:

$$F_1 = \tanh(\Gamma^4) \quad (38)$$

$$\Gamma = \min \left(\max \left(\frac{\sqrt{k}}{\beta * \omega d}; \frac{500\mu}{\rho \omega d^2} \right); \left(\frac{4p\sigma_{\omega 2} k}{CD_{k\omega} d^2} \right) \right) \quad (39)$$

Where d is the normal distance from the wall and $CD_{k\omega}$, defined as follows, being the cross-diffusion term of the model:

$$CD_{k\omega} = \max\left(\frac{2\rho\omega\omega_2}{\omega} \frac{\partial k \partial \omega}{\partial x_j \partial x_j}; 10^{-20}\right) \quad (40)$$

The eddy viscosity μ_T is defined as:

$$\mu_T = \frac{\rho K / \omega}{\max\left(1, \frac{\Omega F_2}{a_1 \omega}\right)} \quad (41)$$

With $a_1 = 0.31$, the value of eddy viscosity is limited forcing the turbulent shear stress to be bounded by the turbulent kinetic energy times a_1 , by using the blending function F_2 and the absolute value of the vorticity Ω [4].

$$F_2 = \tanh(\Gamma_2^2) \quad (42)$$

$$\Gamma_2 = \max\left(\frac{2\sqrt{k}}{\beta * \omega d}; \frac{500\mu}{\rho d^2 \omega}\right) \quad (43)$$

The constants and coefficients of the SST $k - \omega$ model are the following where the coefficients β, γ, σ_k and σ_w denoted with Φ are defined in terms of the coefficients of the original $k - \omega$ and the transformed $k - \epsilon$ models denoted as Φ_1 and Φ_2 respectively.

$$\phi = F_1 \phi_1 + (1 - F_1) \phi_2 \quad (44)$$

Where $\phi = \{\beta, \gamma, \sigma_k, \sigma_w\}$

Table 1: SST $k - \omega$ model coefficients

ϕ	1	2
σ_k	0.85	1.0
σ_w	0.5	0.856
β	0.075	0.0828

And γ is calculated as follows with constant values of 0.41 and 0.09 for k and β^* .

$$\gamma = \frac{\beta}{\beta^*} - \frac{\sigma_w k^2}{\sqrt{\beta^*}} \quad (45)$$

Wall Treatment

In ship hydrodynamics the flows are characterized to be turbulent. Due to viscosity, high gradients are expected near a solid wall of the boundary layer. Thus, generating an appropriate grid is required to correctly capture these high gradients with numerical

simulation.

In **Fig. 6** the structure of the Turbulent Boundary Layer can be seen composed by three regions: viscous sub-layer, buffer layer and the log layer, where the evolution of the dimensionless velocity u^+ can be seen as a function of the wall coordinate y^+ .

$$y^+ = \frac{yu_\tau}{\nu}, \quad u_\tau = \sqrt{\frac{\tau_w}{\rho}} \quad \text{and} \quad u^+ = \frac{u}{u_\tau}$$

Where:

- y^+ is the wall coordinate.
- y distance to the wall.
- u^+ dimensionless velocity.
- u velocity parallel to the wall.
- τ_w the wall shear stress.
- u_τ friction velocity.

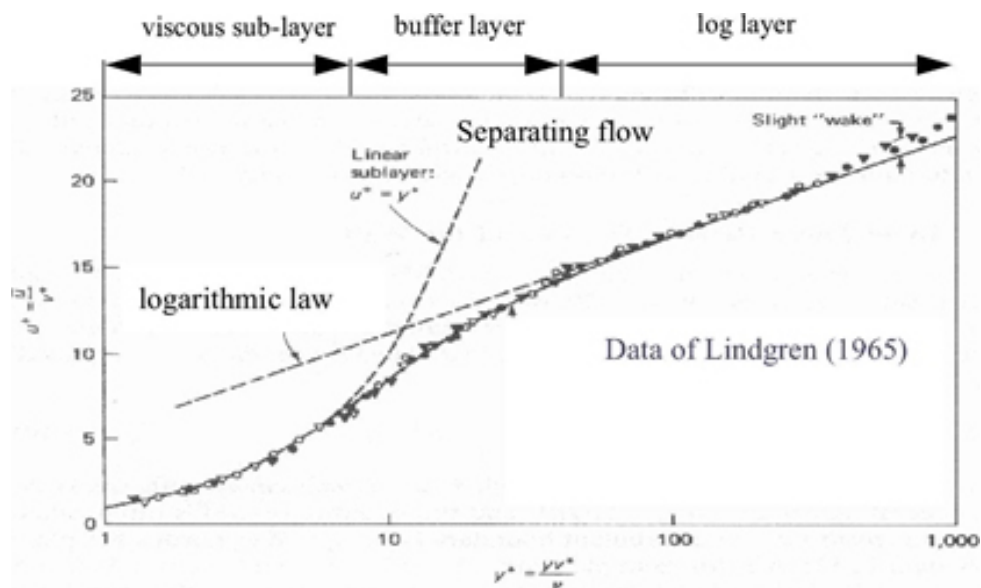


Figure 6: Boundary Layer profiles [4]

Different approaches are considered to solve the boundary layer.

- Low Reynolds models:
Low Reynolds models solve the viscous sub-layer and are well suited when the value of the first node near the wall y_1^+ is below 1. This region is characterized by a linear sublayer function where the wall distance is linear with the velocity profile $y^+ = u^+$.
- High Reynolds models (Wall Function):
The first point is assumed to be in the logarithmic layer $y^+ > 11$ and the velocity is

described by the logarithmic function:

$$u^+ = \frac{1}{k} \ln y^+ + B \quad (46)$$

A slip boundary condition is imposed to the wall $u \neq 0$, appropriate values for y_1^+ are in the range of 30 to 300.

- Two- Layer Approach:

The domain is divided in two regions: the near wall which is affected by the viscosity and the outer region considered as fully turbulent. The separation between regions is defined with the distance from the wall $y^+ \sim 30$.

For all the simulations in this work, the *High Reynolds model (Wall Function)* has been used. The y^+ value depends on the Reynolds number and as a consequence for high Reynolds numbers, higher values can be used. During this work, the ship is modelled at full scale due to higher values which are expected in the range of 30 to 300. Computations were carried out according to recommendations from *Numeca* [4] for the highest velocity considered for the simulation to avoid changes on the mesh.

$$y^+ = \max \left\{ y_{min}^+; \min \left\{ 30 + \frac{(Re - 10^6) * 270}{10^9}; y_{max}^+ \right\} \right\} \quad (47)$$

$$30 \leq y^+ \leq 300$$

3 SHIP MAIN CHARACTERISTICS

The vessel is a Ro-Ro sailing vessel for cargo transportation of various types of cargo: containers, trailers, cars and non standardized cargo.

The navigation area of the vessel is a controlled emission area according to **IMO** regulations [20]. The vessel was designed to achieve the following main goals:

- Reduce fuel consumption and gas emissions.
- Reduce operating costs.
- Reduce the environmental impact of the vessel during all the life cycle.

3.1 Propulsion System

Different propulsion systems have been explored. According to design requirements, the main idea is to select a propulsion system in order to reduce the fuel consumption and the pollution. As a consequence different propulsion systems have been studied, selecting a mixed configuration (Diesel-Electric +Sails) novel propulsion system concept for a cargo vessel.

The operation profile states that the ship will be able to sail using the sails around 90% of the navigation time with or without mechanical propulsion.

3.1.1 Hybrid Propulsion System

Nowadays, propulsion manufacturers are investing on research and development programs finding new solutions for improving the performance, maximizing the efficiency of the systems, and reducing the losses of energy.

The hybrid concept is a system in which the power equipments are fully integrated, and controlled by an **Integrated Control, Alarm and Monitoring System**. The system is composed mainly of the following equipments:

- Controlable pitch propeller (Cpp)
- Auxiliary gensets (GS)
- Energy storage system (ESS)
- Frequency converter unit (FC)
- Main engine (M/E)
- Propulsion control system (PCS)
- Power management system (PMS)
- Reduction gearbox (RGB)

Operation Modes

- PTO: Power Take Off mode in which the shaft machine is providing electrical power to the ship (use or storage).
 - PTI: Power Take In mode in which the ship is at high speed demanding additional power than the provided by the main engine. In this mode, the additional power is given by the auxiliary generators.
-

- PTH: Power Take Home considered as emergency propulsion for the ship when the main engine is out of service, providing the required power to return home using the auxiliary generators.

The PTO operational mode is used when the ship is sailing under mixed propulsion, thereby reducing the fuel consumption from the auxiliary generators and also saving power in the energy storing device. The PTI operational mode is used when the ship has to sail at the maximum speed, taking additional power from the electric generators.

3.2 Skeg design

Initial forms of the hull have been proposed during the concept design of the project. *CFD* calculations based on *ISIS-CFD* solver have been performed for 10 different models comparing the total resistance for three different velocities 11, 13 and 15 knots, and the sway forces for the same velocities considering three different leeway angles $\lambda = 2^\circ, 5^\circ, 8^\circ$. The hull shown on **Fig. 7b** has been defined as the best design and has been considered during the course of this work. For the purpose of this work, the previous studies performed for the best hull form are not mentioned.

However, the skeg of this initial design has to be changed due to additional requirements coming from the Hybrid propulsion system which requires space for electric motor module behind the gearbox and also an additional Aft Thruster, not considered in the initial requirements. Also considering the contribution and importance of the skeg for a sailing vessel in terms of added components of resistance and performance improvement for course stability and balance of forces.

Based on the minimum distances to be kept between the main components of the system and the hull, four different skegs were designed in order to compare their influences on the resistance in calm water and the sway forces and resistance for a leeway condition.

The minimum distances to be kept from the center line \mathcal{C} to the hull can be seen in **Table 2**.

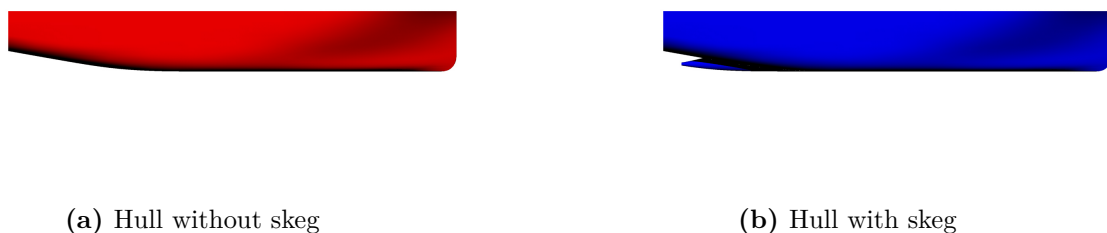


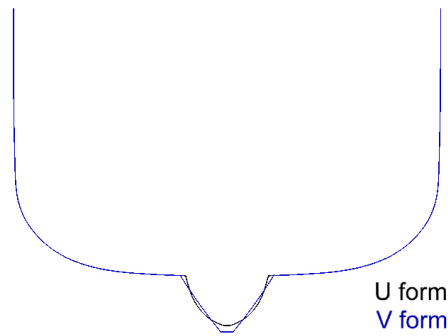
Figure 7: Initial hulls concept design

Table 2: Distance constraints

Main Engine aft (m)	1.9
Gearbox (m)	1.5
Aft thruster (m)	0.75

As mentioned earlier, the goal is to compare the resistance and lateral forces between the different forms and to define the best shape in terms of hydrodynamic performances, while satisfying all the design requirements.

Two main types of skeg forms have been proposed with round (U) V1 and straight V2 (V) forms. From these two skeg forms, modifications were done, in order to check the influence of the shape (V and U) while maintaining the same lateral area V3 and V4.

**Figure 8:** U and V skeg forms

4 INITIAL CFD CALCULATIONS

In this chapter, the first CFD calculations have been performed in order to compare the performance of the different models on different conditions and different sets velocities $V = \{8, 10, 12, 13, 14, 15\}$ knots for the load condition of 10500 tons. All the simulations in this chapter were ran on a high power computation cluster of 64 cores/128 threads @2.9GHz with a total of 360 hours of computation time.

All the simulations were done just for the hull with the proposed skeg, but without additional appendages. The contributions for the resistance of these additional components had already been provided during the concept design with a value of 5%.

The first simulation is a resistance study, in order to measure the total resistance and BHP required for the given velocities and to compare them with the trial velocities defined on the technical specifications. For this simulation, two mesh sizes (fine and coarse) were selected in order to compare the sensitivity between the different models to mesh size. However, similar behaviour are expected between the different models. It is better to use coarse mesh at the beginning of the design stage in order to reduce the computation time and also giving promising results. With the coarse mesh, it was able to define which design amongst others is best to study on detail. The second simulation was also a resistance study for the same velocities, considering a leeway angle $\lambda = 5^\circ$. For this sailing vessel, examining the added resistance and the sway forces are of paramount importance, and, therefore, were considered in the second simulation.

4.1 SIMULATIONS SET-UP

4.1.1 Mesh generation

In order to firstly set properly the grid, the domain of the simulation has to be defined. The domain was defined following the guidelines from **ITTC** [9]. The boundaries have to be placed sufficiently far from the ship, in order to avoid their influences on the solution. In **Fig.9** the domain for both simulations can be seen. For the condition without leeway angle, the symmetry can be defined due to the symmetric conditions of the flow reducing significantly the size of the domain. However, for the leeway condition, the symmetry condition can not be defined due to the non-symmetric condition of the flow.

The hull is composed of different regions in order to define boundary conditions and refinement regions where the flow has to be solved in detail, such as the skeg and regions with high curvatures. All the submerged regions and in contact with the high density fluid (water) are defined as Wall Boundary condition (Wall Function), as mentioned in **Sec.2.4.2**. The deck, which is in contact with the low density fluid (air), is defined as Slip Wall with zero stress at the wall neglecting the turbulence due to shear.

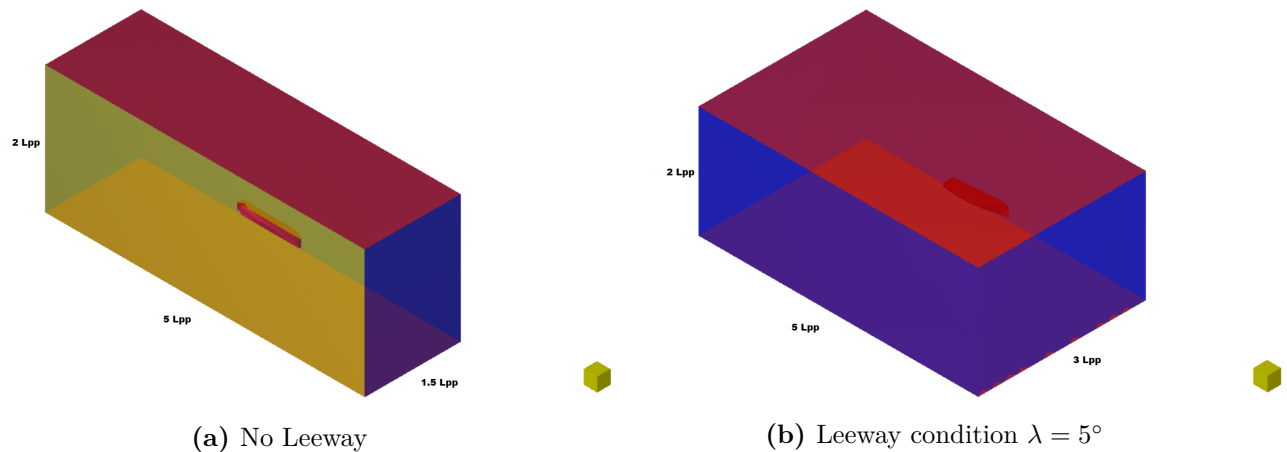


Figure 9: Domain of the simulation

On the external boundaries of the domain, the conditions have to be imposed. As mentioned earlier, for the simulation without leeway, a symmetry condition has been imposed restricting the simulation to one half of the domain, due to the presence of tangential velocity to the mirror plane. For both cases, the top and bottom boundaries were defined as prescribed pressure, which updates the hydrostatic pressure with the position of the free surface during the simulation. The remaining external boundaries were defined as Far field, making it possible to prescribe values for the velocities, mass fraction, and turbulence. In this type of boundaries the flow is going inside or leaving the domain. For this case study, the velocity is imposed to the ship, and, considering that the resistance study is in calm water, no velocity is imposed on the boundaries.

Once the domain and external boundaries are defined, an unstructured hexahedral mesh is performed using five different steps:

- **Initial mesh:** In this step, a very coarse mesh is automatically created along the domain in order to define the size of the cells for the far field.
- **Adapt to geometry:** Refinement of the initial cell has been performed. In order to better capture the flow in some regions, different curve, surface and volume refinements have been carried out with focus on the skeg, hull, and free surface. After the refinement, the trimming process is performed by removing all the cells intersecting or located outside the geometry. As a result, a staircase mesh is obtained.
- **Snap to geometry:** In order to improve the quality of the body, the mesh was projected to the surface to recover geometric features.
- **Optimize:** Once the snapping process is performed, poor quality cells are obtained. They are usually located close to the curves and corners. In this step, an automatic optimization of the mesh is performed in order to improve the quality of the cells by slightly displacing their vertices and avoiding concave and negative cells thereby improving the orthogonality of cells.

- Viscous layer insertion: To properly capture the viscous layers, prism layers with high aspect ratio are inserted to the cells and connected to the walls. As mentioned on **Sec. 2.4.2** the viscous layer insertion has been performed following the recommendations from Numeca according to **Eq. 47** for the highest velocity, so as to obtain a value of $y^+ = 287$.

In **Table. 3** the obtained number of cells for the different simulations can be seen. For all the meshes, the same parameters were defined and volume refinements have been performed around the skag, so as to better capture and determine the influence of the different forms. The difference in the number of cells between the different models, is due to the variation on the geometry, and as a consequence different number of cells are expected even with the same parameters.

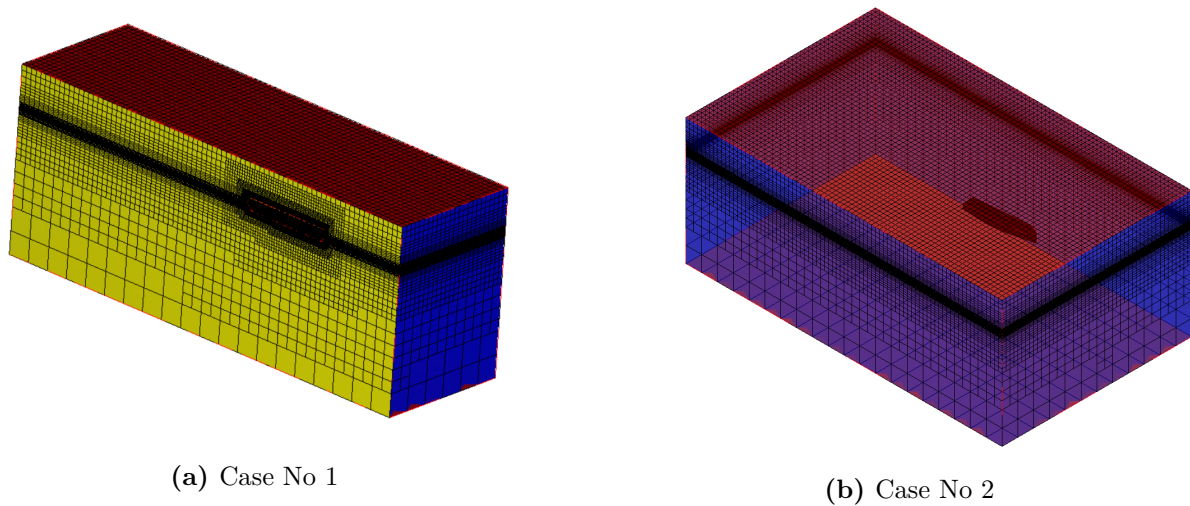


Figure 10: Mesh Version 1

Table 3: Number of cells different meshes

	Number of cells		
	Condition No 1		Condition No 2
	Coarse	Fine	Fine
V1	710.542	1'912.652	3'850.245
V2	773.256	1'925.248	3'899.579
V3	747.909	1'935.436	3'892.512
V4	715.489	1'920.045	3'889.171

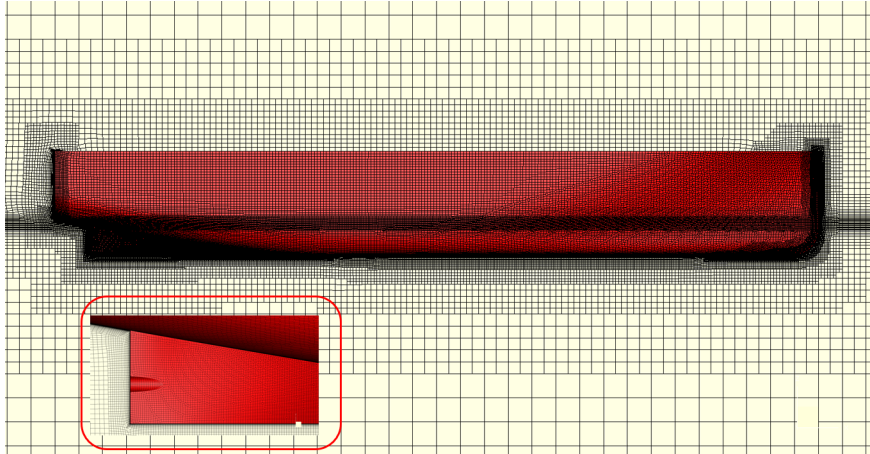


Figure 11: Mesh Details Version 2

4.1.2 Flow settings

The additional set-up of the simulation is mainly divided into two parts: *Physical configuration*, in which all the motion and flow settings are defined; and the *Computation control*, where the numerical parameters and outputs are selected.

PHYSICAL CONFIGURATION

Initially, a multi-fluid model is selected and the properties of the salt water and air are defined. In order to solve the viscous effects, the turbulence model $k - \omega$ *SST-Menter* explained in detail on **Sec.2.4.2** has been utilized.

Body Motion

- Motion Definition

Three degrees of freedom are considered. For the resistance prediction in numerical and experimental fluid dynamics, T_X0 (surge) is imposed, T_Z0 (Heave) and R_Y1 (Pitch) are solved. In order to reach the defined velocity, a motion law has to be implemented. The absolute 1/2 sinusoidal ramp profile is selected. With this method the acceleration of the body is controlled and the velocity is incremented according to this function and attaining the defined value on a final time t_1 inputted by the user. For this case, time corresponds to 1/4 of the simulation time.

- Dynamic Parameters

In order to find the position of the body when the solution of one or more degrees of freedoms is required, the solver solves the Newton's second law of motion based on inertial properties.

$$m \frac{d\vec{v}}{dt} = \vec{f} \quad (48)$$

When the rotations of the body has to be solved, the definition of the inertia matrix and it's components are required in the reference frame of the body.

- External Forces

In order to properly simulate the towing force, the Drag Based Wrench option is selected by defining the point of application of the force in the Cartesian coordinates of the gearbox.

COMPUTATION CONTROL

- Adaptive Grid Refinement

In order to properly capture the flow, this criteria has been proposed by *Wackers* [23], which significantly reduces the number of cells and improves the quality of the solution, by refining the cells during the simulation in specific areas where the flow is changed like breaking waves, appendages in which vortices are created or the wake. The Free Surface Directional criterion has been selected, this criteria is specially used to correctly capture the free surface when it is parallel to the grid generation, a refinement around the water normal to the surface is implemented.

- Time step law

To define the time step, the uniform law is selected in which the time step is constant for all the simulation, and it is expressed in terms of the reference length and velocity. The selected value is $\Delta t = 0.08s$ for all the simulations.

4.2 RESISTANCE AND POWERING

4.2.1 Case 1: No leeway

Resistance Comparison: Coarse and Fine Mesh

The first resistance calculation was performed for two different meshes as defined in **Table 3**, in order to determine the sensitivity in the results for the different models, with the purpose of identifying if, for successive projects, it is viable to reduce the number of cells of the mesh, especially when different models have to be tested. Expecting a considerable difference on the results between the fine and coarse mesh of each model, but a similar behaviour between the different models.

There is a significant error between the coarse and fine mesh for all models around 4%. As a consequence, finer meshes are required for detailed studies. However, it can be noticed that the coarse mesh provides a good comparison between the different models reducing the computation time for preliminary studies. The round (U) forms V1 and V4 has lower resistance compared to the straight (V) forms V2 and V3. For both meshes V1 has the

lower resistance, followed by V4, V3 and V2 respectively. Taking as a reference the model with less resistance V1, absolute errors has been calculated in order to determine the additional resistance induced by the other models as can be seen on **Fig. 12** with less than 0.5% for V4, around 2.5% for V3, and around 4% of additional resistance for V2.

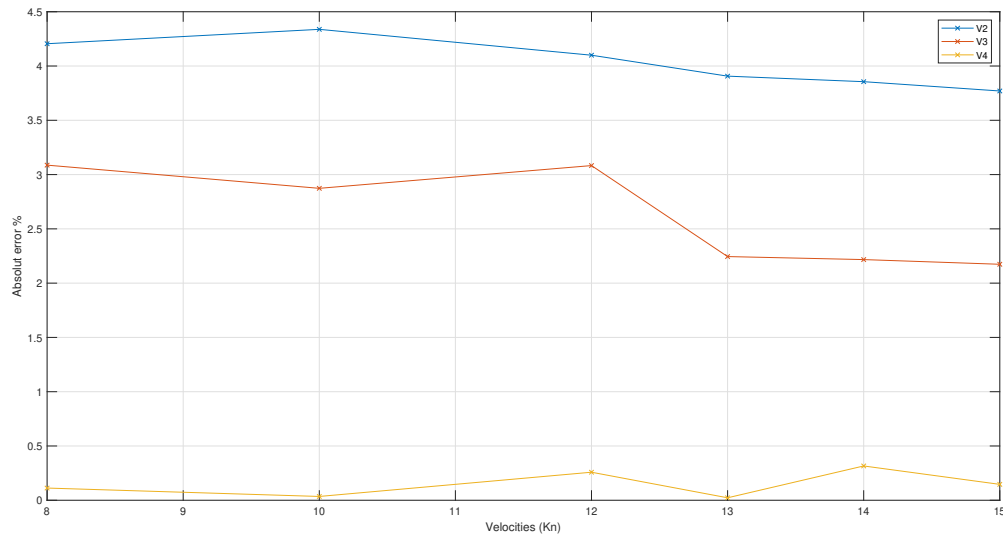


Figure 12: Absolute error Resistance Case No 1.

Due to limitations in computation power, no additional mesh convergence studies was performed, and the results from the fine mesh are considered as good results.

Efficiencies

As mentioned in **Sec. 2.2.2**, the wake field is different for all ships. This is influenced by the following: the streamline flow around the body, boundary layer, and wave making effects. In **Fig. 13** the difference between (U) and (V) shapes can be seen. Comparing V1 and V2, for (V) forms the axial velocity of the flow on the propeller disk is higher. However, in the top and bottom location at the, center the reduction of the velocity is considerable generating even reverse flows. For (U) forms it is noticeable that the flow is not able to follow the curvature of the skeg. Therefore the flow separates from the hull surface [8].

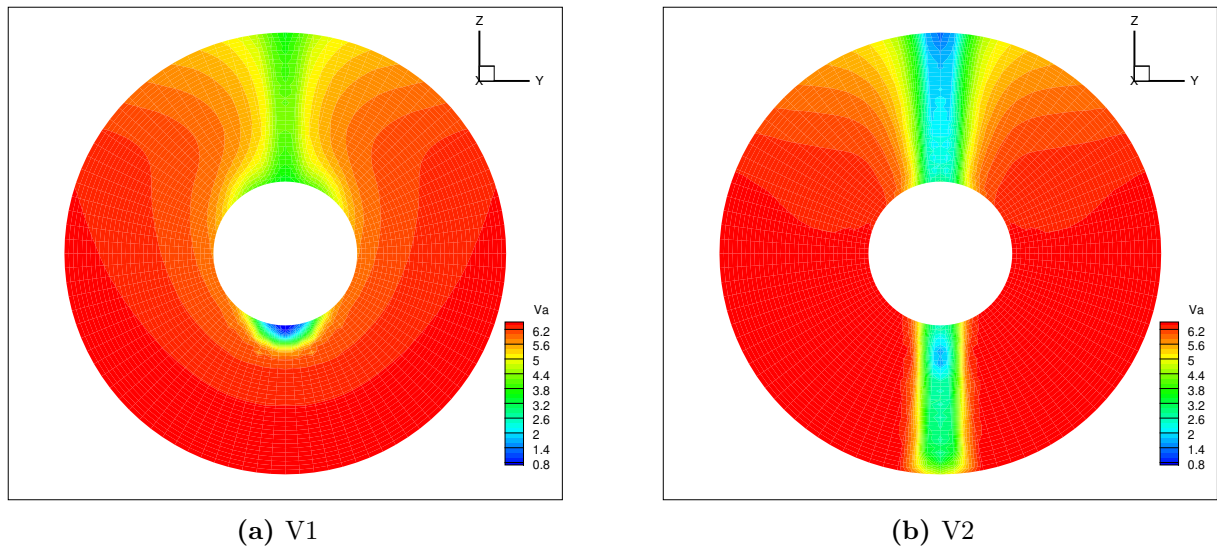


Figure 13: Wake Flow 14 Kn

Once the results from this simulation are obtained, the efficiency of the hull can be computed and analyzed based on **Equation 6**.

The additional efficiencies mentioned previously involved in the propulsion system are not dependent on the hull form. The values of these efficiencies and the overall propulsive efficiency is displayed in **Table. 4**.

Table 4: Efficiencies propulsion system

	V1	V2	V3	V4
η_H	0.97	0.98	0.94	0.99
η_0		0.60		
η_S		0.97		
OPC	0.57	0.57	0.55	0.58

Total Resistance and Powering

In order to obtain the total resistance and powering, additional values to the obtained resistance from this work have been considered. By taking into account all the components of the resistance, the added resistance due to the appendages and the air resistance must be considered. Also, a margin of 4% is taking into account. The mentioned additional components of the resistance were computed before of the project for all the velocities of this study and, therefore, just the values are added to the total resistance.

According to the technical specifications the ship has to be tested on calm deep water with a clean hull and without the anti drift fins for two velocities:

- 13.8 Knots at 100% MCR of the main engine and without the electric booster (PTI).

- 14.8 Knots at 100% MCR of the main engine and with the additional power provided by the electric booster (PTI).

From the obtained results of the total resistance for all the test velocities, it is possible to determine the required delivered power of the engine (BHP) for all the velocities. This design step is highly important in determining if the design fulfills the performance required by the client, and to accomplish all the requirements before the construction of the ship together with good results during test trials. This delivered power can be calculated from **Eq. 9**.

In **Fig. 14** the speed power estimation curve is displayed and it can be noticed that all the models satisfy the requirements regarding the velocities of 13.8 Kn and 14.8 Kn for the sea trials. In general, the (U) shape models have the lowest power requirements for all the tested velocities. With the model V4 the best performance for resistance prediction on calm seas without considering leeway, it requires around 2%, 4% and 7.6% less power compared with V1, V2 and V3 respectively.

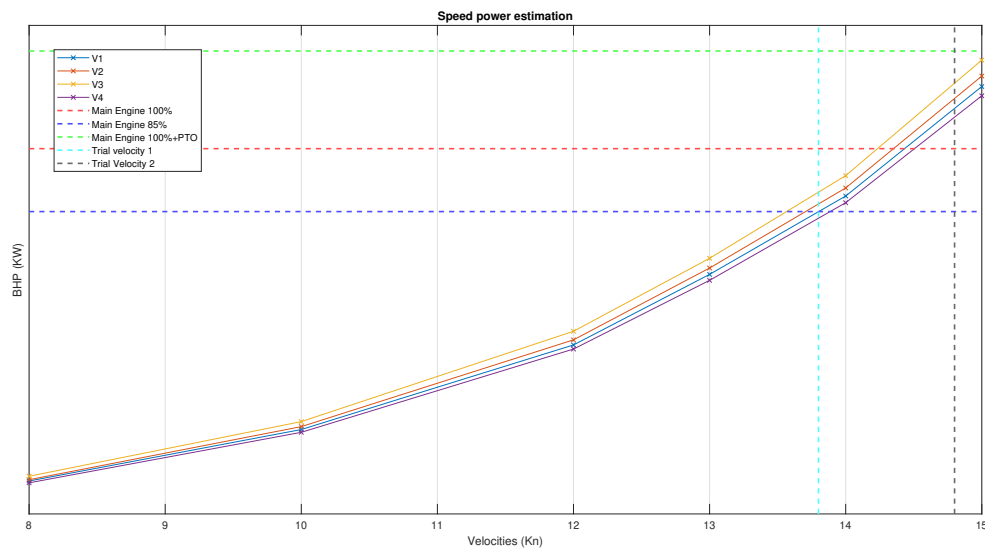


Figure 14: Power- Speed estimation

4.2.2 Case 2: Leeway Condition

Additional aspects must be studied in order to define the best model for a sailing vessel. As explained in **Sec. 2.2.2** the total resistance of a sailboat has additional terms due to the change in the resistance imposed by the heel angle (ϕ) ΔR_{Rh} , leeway angle (λ) ΔR_{RK} , and the induced resistance, due to the side force generation. For this condition the study is not only focused on the impact of the different models on the resistance, but also the side forces are considered. This will significantly improve the performance of the vessel on

sailing condition for course stability, and to balance the forces applied due to the action of the wind on the sails.

As stated earlier, the flow in this condition is not symmetric. Therefore, the full domain has to be modeled, thereby, consequently increasing the number of cells and the computation time.

Previous studies have been performed for the same ship by considering different heeling (ϕ) and leeway (λ) angles for the initial hull without skeg shown in **Fig 7a**, and the hull with skeg in **Fig. 7b**, in which the resistance and side forces were analyzed.

In this thesis, in order to reduce the computation time, just one leeway angle was studied for all the models, no mesh convergence studies were performed, and the simulations were performed for the same velocities as the previous section with a leeway angle $\lambda = 5^\circ$.

Resistance Calculations

For this condition, the aim is to compare the induced resistance by the leeway angle and side forces. As a consequence, no additional components of the resistance were considered, also the required power was just considered for the sea trials (not sailing condition).

Similar results were obtained for the resistance, with higher values for the hulls with (V) forms (V2 and V3), and less resistance for (U) forms (V1 and V4). V1 model had the lowest resistance followed by V4, V3 and V2 with additional resistance of around 0.8%, 6.2% and 8.6% respectively.

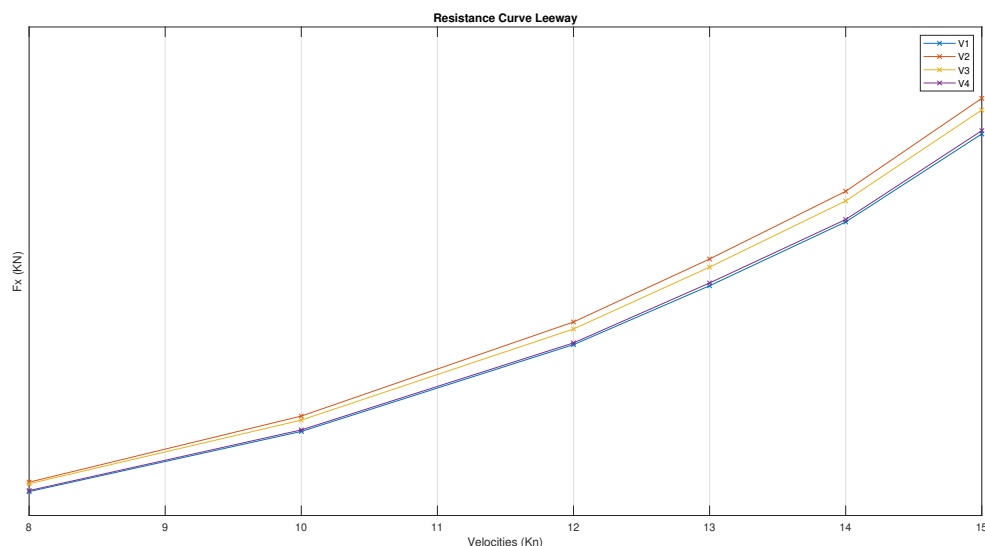


Figure 15: Resistance curve Condition No 2

Sway Forces- Lateral Forces

For sailing boats, one of the design criteria is to increase the lateral forces exerted by the hull and all the appendages. This lateral force is the hydrodynamic force to compensate

the forces applied by the wind on the sails to attain equilibrium. Also, as mentioned earlier, they contribute to the course stability of the vessel which is an important factor to take into account.

Significant contributions on the lateral forces can be seen from the different models of the skag, the forms with (V) shapes highly increase this forces. It is important to consider the differences on the lateral area of the different models. An increment in the lateral area directly influences the sway forces exerted by the hull. As expected, the contribution on the lateral forces of model No 2 is significant around 70% more compared with the lowest model V1. From models V3 and V4 it can be confirmed the contribution of the (V) forms considering that the two models have the same lateral area. However, V3 has around 47% high contribution to the lateral forces, and V4 with 16% from the lowest V1. The mentioned differences can be seen in **Fig. 16**.

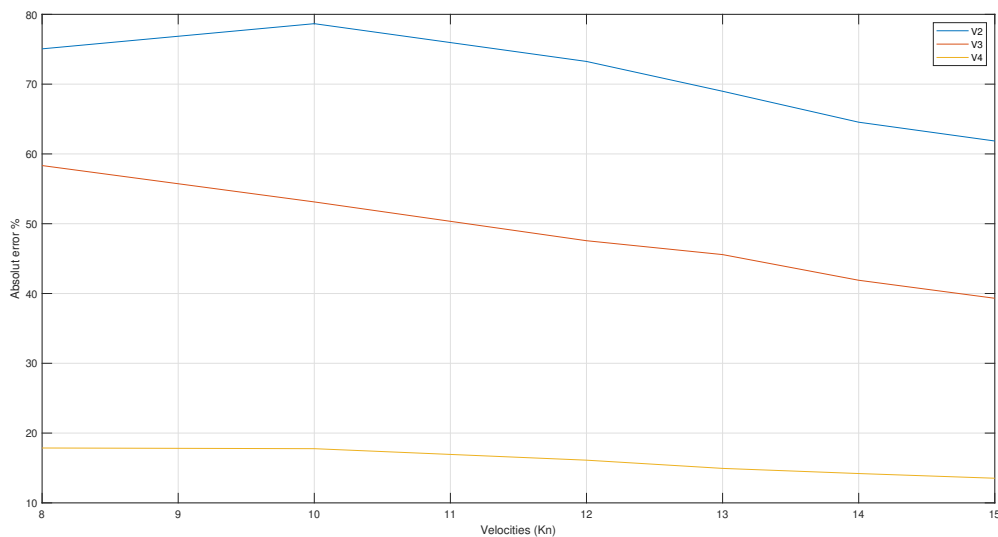


Figure 16: Difference Sway Forces $\lambda = 5^\circ$

To have a better idea of the sway forces from the different hulls, the sway forces by sections have been analyzed. In **Fig. 17** the sway forces by sections are displayed, these forces are taken at 100 points along the length of the hull with a distance of 1.36m between each section. The influence of the (V) forms can be observed. However, from this figure it can be seen that the high value obtained on V2 was due to the lateral area of the skag, which is continuous until the propeller location. The reduction on the other models compared to V2 is due to the non-continuous lateral area of the skag.

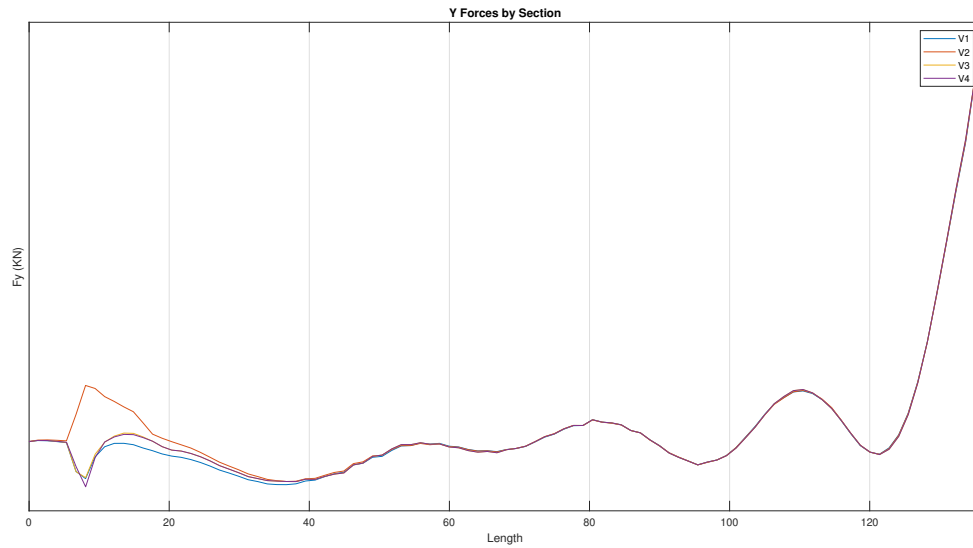


Figure 17: Sway Forces by Section

Additional anti drift appendages are considered during the design of the ship, being equipped with two retractable anti-drifting fins, see **Fig.18** in order to improve the performance of the ship when it is being propelled by sails. The lift produced by the fins of this ship was studied in another Master Thesis with some time prior to the present work [2]. The lift and drag induced by the fins were measured for different leeway (λ) angles at different velocities for two types of fins. The lift depends on the lifting coefficient C_L , area A in m^2 and the velocity.

$$L = C_L \cdot A \cdot \frac{\rho u^2}{2} \quad (49)$$

In order to compare the lift produced by the fins with the different forms of the skeg, only the results of $\lambda = 5^\circ$ at 11 Kn have been considered for the two different types of fins and the rudder.

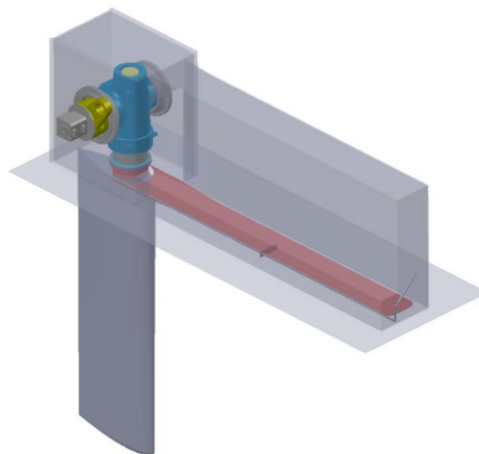


Figure 18: Anti-drift fins [2]

From the previous studies [2] and the obtained results from this work, the contribution to the total side forces of the vessel from the different skeg models can be deduced considering the sway forces of the bare hull for leeway angle $\lambda = 5^\circ$ and 11Kn of velocity.

4.2.3 Analysis and Results

In order to define the appropriate model with respect to the design requirements of the ship. The obtained results from **Sec. 4.2.1** and **4.2.2** have been analyzed with the purpose to get better agreement between the required power of the ship for all the range of velocities and also to reach a good performance when the ship is propelled by sails or mixed propulsion configuration.

It can be seen from **Fig. 14** that the model No 4 has the highest overall propulsive coefficient *OPC*, and less requirements in terms of powering, with a reduction of about 2%, 4% and 7.6% from models No 1, No 2 and No 3 respectively. From **Fig. 15** a similar performance can be observed as lower resistance for the skeg with (U) shapes was obtained. The model No 1 had the lowest induced resistance due to leeway (λ), with less than 1% from model No 4. However, higher values of 8.6% and 6.2% were obtained for models No 2 and No 3 respectively.

Regarding the sway forces, it was noticed that the skegs with (V) shapes increased significantly the forces. However, considering the contributions to the lateral forces of all the appendages, especially the contribution of the two analyzed anti-drifting fins and the rudder, the difference in the contribution of the skeg to this forces is not relevant between the different models.

With regards to the just stated analyses, the model No 4 was selected, having the best agreement with a reduced resistance and powering and good contribution to the lateral forces. This model is used for the resistance optimization in the next chapter.

5 HULL OPTIMIZATION

The optimization of the hull was carried out with the environment of *Friendship Systems "CAESES"*. In order to reduce the computation time used during the optimization, the process was performed in two different phases on a 4 cores/8 threads @2GHz with 207 hours of computation time. Firstly, an optimization of the forward part of the hull was carried out using a multi-objective optimization algorithm for the two trial velocities by optimizing the wave resistance coefficient C_w with Potential Flow theory. Based on the optimized hull from the wave resistant coefficient a single objective optimization was carried out for 14 Kn using the *Zonal Approach* by considering the viscous effects on the stern and wake flow.

5.1 SHIPFLOW STRUCTURE

The *CFD* solver *Shipflow* is a special purpose code developed for *Naval Architecture*. One of the benefits of this software is the high computational efficiency, being able to get accurate results using low computation power, and requiring few *CPU* hours for a simulation.

This solver use the *Zonal Approach*, where the flow is divided into three different zones with different solution methods. The basis for the division of the flow is *Prandtl's* finding that the viscosity, although is present in the entire flow field, plays part only in a thin layer around the body and behind it, thereby making it possible to use the *Potential Flow Theory* in the outer flow "Zone 1", the *Boundary Layer Method* in the thin boundary layer "Zone 2" and *RANS* equations at the stern/wake flow "Zone 3" [16].

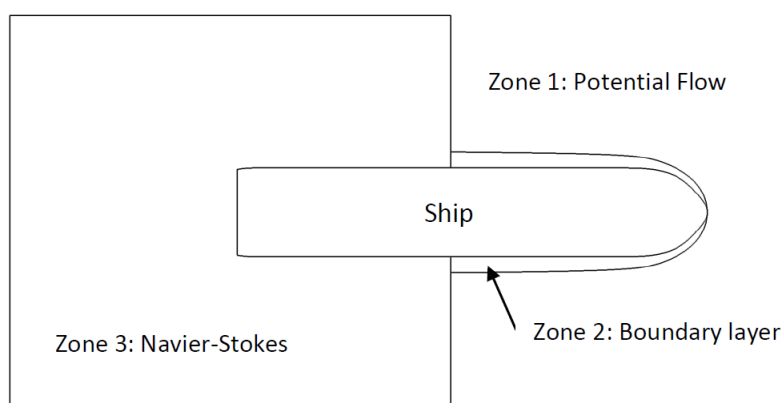


Figure 19: Zonal- Approach *Shipflow*

Another advantage of the zonal approach is the prediction of the free surface flow with *Potential Flow Theory* computed with a reasonable time compared to *RANS* equations, in which the solution is time-dependent with many time steps. However, this reduction

and simplification of the approach has an impact on the solution some how in which the lift and the wave field in the stern is over-predicted due to the neglected effects of the viscosity.

Shipflow has three different modules **XPAN**, **XBOUND** and **XCHAP**. Depending on the requirements of the user, one, two or all the modules can be used together.

- **XPAN**: Is the flow solver for the Potential Flow around three dimensional bodies, based on a surface singularity panel method.
- **XBOUND**: Is the solver for thin boundary layer computations. It is based on streamlines automatically traced from the potential flow solution. The momentum integral equations for boundary layer are solved along this streamlines. This module is capable of computing the laminar boundary layer and the transition to the turbulent boundary layer.
- **XCHAP**: Is a *Finite Volume* based solver that solves the *RANS* equations using different turbulence models. This solver can be used in a Zonal or Global approach.

The geometry has to be imported on ".igs" file format to the *CAESES* environment. In order to continue with the generation of the panels for the potential flow module, the geometry must be transformed into an offset file in which the geometry is well defined and used for the generation of the mesh by *XMESH* module. Once this transformation is done, the coordinate system from the offset file is transformed to the Shipflow coordinate system. In which the origin is at the FP *xori* in the longitudinal direction and in the vertical direction at the location of the free surface *zori*.

Most of *CFD* solvers use the *RANS* equations on the entire flow field as in **Chapter. 4**, in which the domain size is highly increased. By using this approach the computational domain in which *RANS* equations are used start from midships and the domain is extended to one hull length downstream and only half of a ship length radially [16].

5.2 PARAMETRIC MODELLING OF THE HULL

In order to perform the optimization, the shape has to be defined with some control parameters, thereby enabling the automatic variation of the shape during the process. The hull can be modified with a semi-parametric or fully parametric approach. The barehull from **Fig. 7a** has been imported on ".igs" format to the *CAESES* environment and the skag was modelled on a fully parametric way based on the shape obtained from model No 4.

5.2.1 Semi - Parametric approach

This approach uses the existing hull and also some transformations to obtain the new hull. As a result, the new geometry has some characteristics related to the previous form.

Different transformations can be used on this approach:

- Merging/morphing: The new hull is produced by the combination of two or more shapes.
- Box deformation: A deformation is applied to the deformation box. The parent shape is placed into this deformation box being distorted by the applied transformation.
- Swinging/shifting: On this transformation the sectional curve area of the hull is changed moving the sections longitudinally. One traditional transformation of this type is the Lackenby transformation method proposed on 1950 by H. Lackenby [15].

This approach is used for the fore-body optimization, using the Lackenby method by considering that a significant variation of the bare hull directly influences the stability and general arrangement of the ship, which was already defined and with small range of variation.

5.2.2 Fully- parametric approach

On this approach, the geometry is modelled based on some parameters, being able to define the surfaces based on longitudinal curves and curves representing the sectional area. By using this approach, the geometry can be highly deformed, creating curves and surfaces with excellent fairness. This approach was used to model and adapt the skeg obtained from **Fig. ??** in order to perform the optimization of the skeg using the *Zonal Approach*.

Skeg modeling

The geometry modeling is based on the definition of parametric curves and the generation of surfaces from them. The skeg was modeled based on six different fully parametric curves describing the geometry (see **Fig. 20**). The parameters are defined in order to make three types of variations on the geometry (see **Fig. 22**).

Positional: The longitudinal and transverse position of some control points is defined based on the following parameters:

- Skeglength: Defining the total length of the skeg (m).
- xAftskeg: Define the starting position of the skeg on the longitudinal direction.
- xFwdskeg: Define the end position of the skeg on the longitudinal direction.
- xMidskeg: Is a control point defining the longitudinal position of the maximum width of the skeg.
- xShaft: Longitudinal position of the shaft.
- zShaft: Defining the vertical position of the shaft center.

Integral: Parameters to define particular areas or volumes of the geometry.

- Skegwidth: Defining the width of the skeg and is used on the curves to control the section area varying the distance of control points from the \mathcal{C} .
- yMaxskeg: Maximum value of the width of the skeg. This parameter is related with xMidskeg.
- Shaftdiameter: Define and control the area of the shaft at the start of the skeg.

Differential: Variations to define the curvature, slopes or angles of the curves.

- Tangentstart: Change the angle at the end of the skeg in the z plane.
- aftTanskeg: Change the angle at the start of the skeg in the z plane.

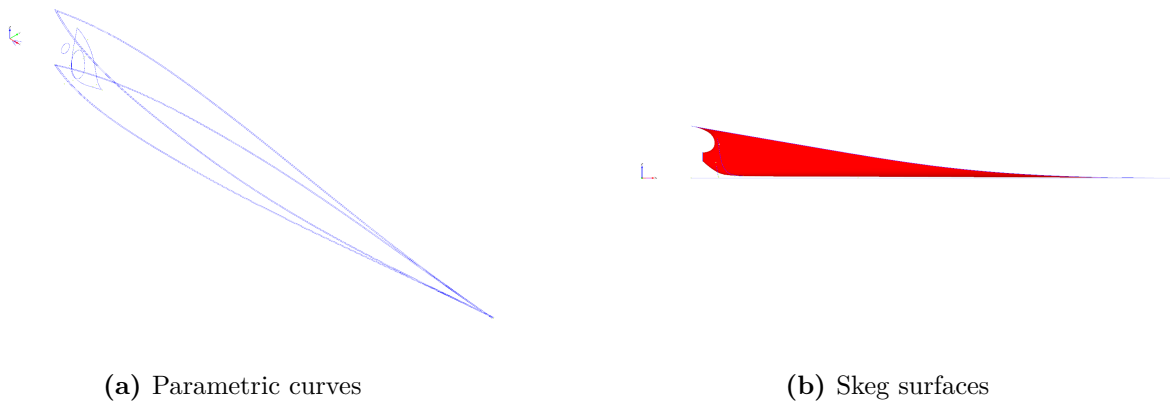


Figure 20: Fully- parametric skeg

Additional control points are defined to apply constraints during the optimization of the skeg, in order to satisfy the minimum distances from the Aft thruster, Gearbox and Main Engine to the skeg as can be seen on **Fig. 21**.

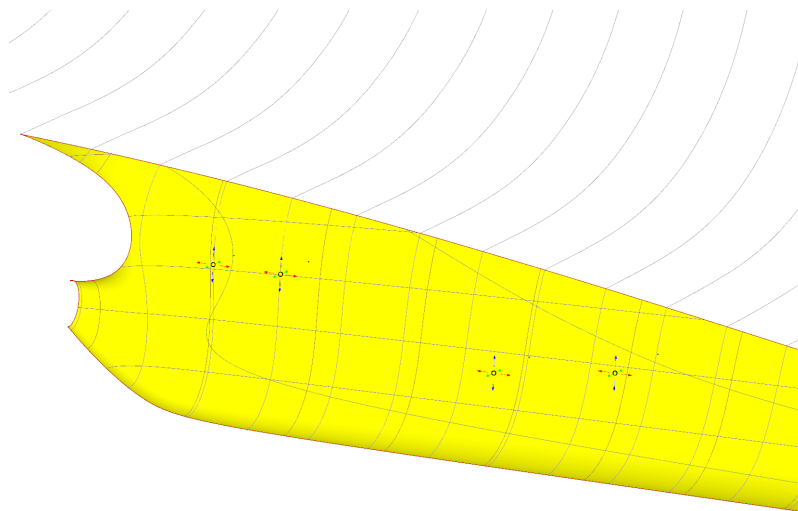


Figure 21: Zonal- Approach *Control points*

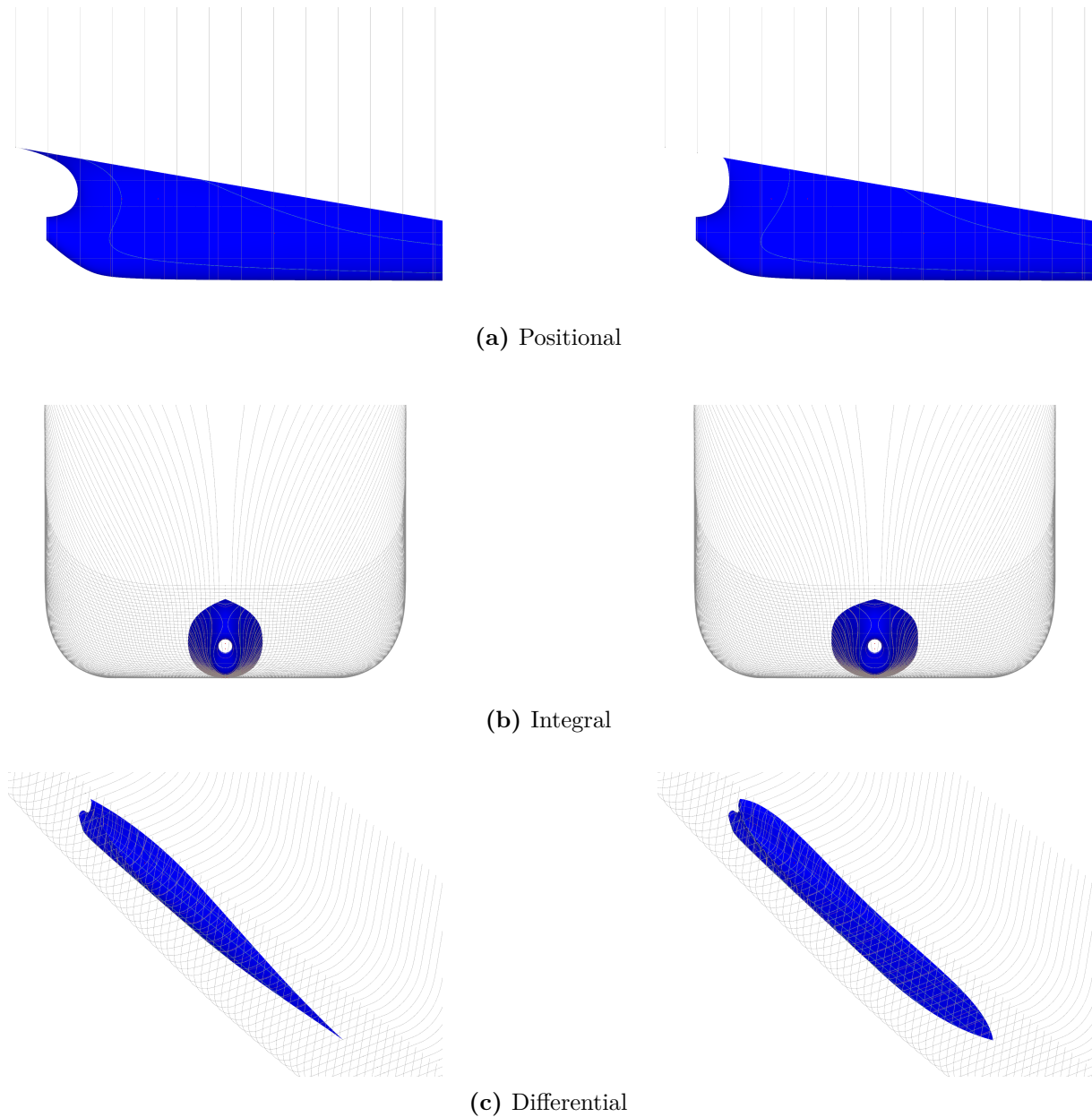


Figure 22: Skeg transformations Fully -parametric approach

5.3 FORWARD OPTIMIZATION - POTENTIAL FLOW

5.3.1 Mesh Convergence Study

The discretization of the domain is one of the most important aspects on the calculation of the wave resistance, which has a strong influence on the quality of the results and on the computation time required during the simulation. Three different meshes were tested in order to get good results, but also with the purpose to reduce the computation time during the optimization. The panelization of the hull depends on the geometry. For complex shapes, more panels are required to correctly represent the surfaces. For these type of hulls the number of panels on the submerged area must be greater than 10 to 12 on the vertical direction Z (points) and 30 to 40 on the longitudinal direction X (stations) [10].

The hull is divided into three sections; the hull, aft part of the skeg and the stern. Three different discretizations of the hull are considered as can be seen in **Fig.23**, where the discretization of the submerged area is displayed.

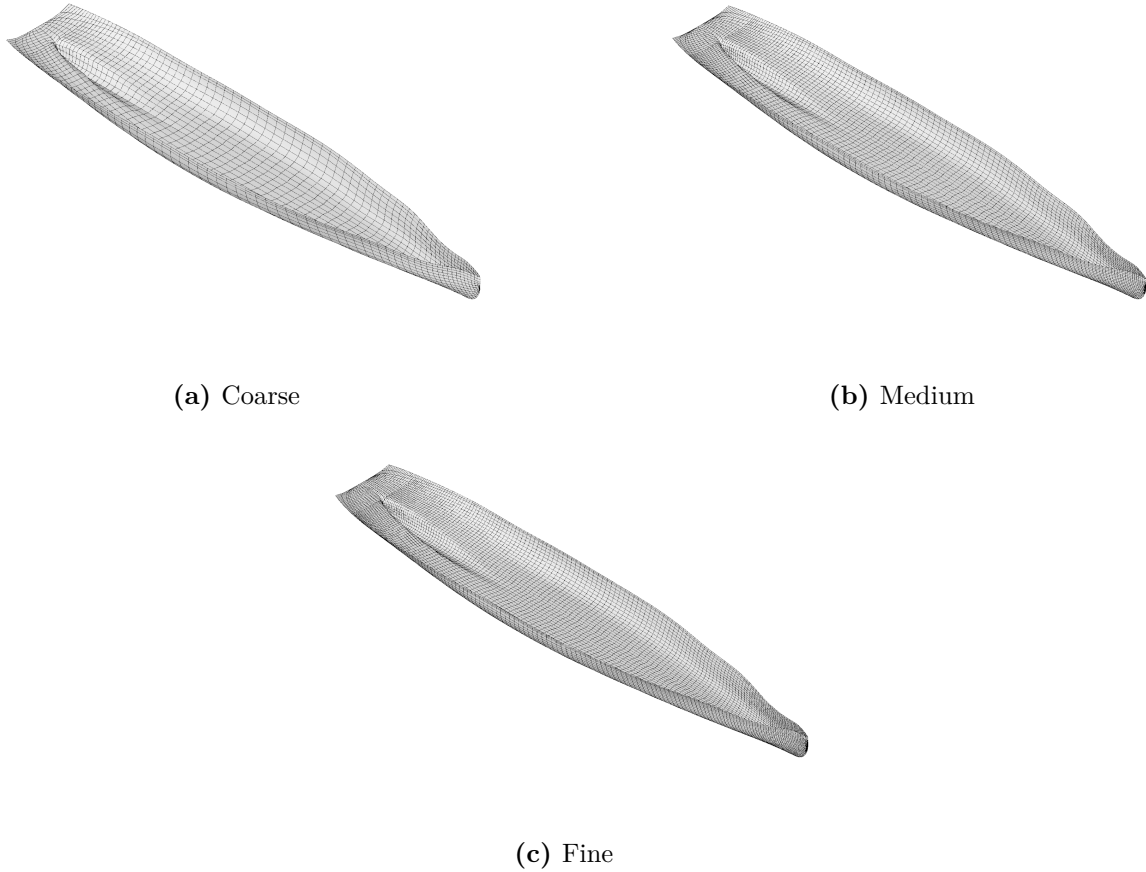


Figure 23: Fully- parametric skeg

The accuracy of the results is also dependent on the discretization of the free surface. The recommended number of panels in the longitudinal direction is minimum of 30 per wavelength (λ), which is computed according to **Eq. 50**.

$$\lambda = 2\pi L F_n^2 \quad (50)$$

A mesh convergence study was carried out considering the variation of the wave coefficient between the different meshes. As a result, the medium mesh was selected having the best agreement between the computation time and the quality of the results with a difference of 3% with respect to the fine mesh and also satisfying all the guidelines from *Shipflow*.

Table 5: Discretization of meshes

Mesh	Number of panels	Number of nodes
Coarse	3644	3930
Medium	9192	9643
Fine	14460	15024

**Figure 24:** Comparison coarse and medium mesh

5.3.2 Multi- Objective Optimization

In this subsection, for this part of the optimization process based on potential flow, a multi objective genetic algorithm was selected. These type of algorithms ensure the convergence of the solution to a global optimum. They are also expensive in terms of computation time, requiring many evaluations of the objective function to reach convergence. It was used in this stage of the optimization considering low requirements in terms of computation power for a potential flow solver.

Transformation Method

The Lackenby [15] transformation is a swinging semi-parametric method widely used by Naval Architects for hull variation based on a parent form. The variation of hull forms based on this method are done according to four parameters:

- Variation of the prismatic coefficient ΔC_P .
- Longitudinal shift of the center of buoyancy ΔX_{CB} .
- Change in the forward position of the parallel mid-body ΔL_{PE} .
- Change in the aft position of parallel mid-body ΔL_{PR} .

The main input of this transformation is the sectional area curve "SAC" which provides information about the center of buoyancy and the displacement. This transformation is a classical distortion based on a constrained transformation function expressed by a first or second order degree polynomial. The transformation functions are formulated and applied to the parent "SAC" thereby deriving the new required "SAC" [15]. The shift functions on this method are applied to both half-bodies up to the forward (FP) and the aft perpendicular (AP).

However, this method has two main drawbacks for the Naval Engineer who sometimes just wants to apply transformations to special regions and the impossibility to change the slopes at the end or the beginning. Based on this method, a new transformation was proposed by Claus Abt and Harries [5]. The Generalized Lackenby in which the transformation can be applied to special regions without modifying the whole hull, also making it possible to define the slopes at the beginning and at the end of the hull, thereby avoiding squeezed or stretched waterlines. This method is based on fairly B-Splines curves instead of the quadratic polynomials [5] (see **Fig. 25**) for detailed description.

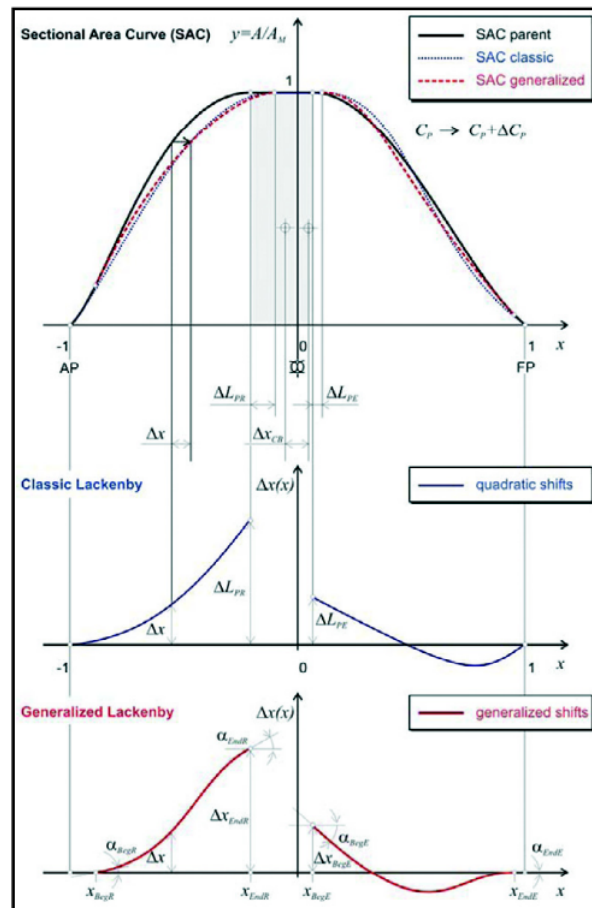


Figure 25: Classic Lackenby and Generalized Lackenby method [5].

This *Generalized Lackenby* transformation was applied for the aft-body optimization by defining the starting point at $0.5 L_{pp}$ up to the (FP). A general view of this transformations

is displayed in **Fig. 26** where a variation of the prismatic coefficient is defined as $\Delta C_p = 0.05\%$. The parent and the modified hulls can be seen with their sectional area curves. The parent form in red and the modified with the displayed offsets.



Figure 26: Generalized Lackenby representation

SAC Optimization

Two objective functions were considered for the optimization of the forebody; the wave resistance coefficient C_w for 13 and 14 knots in order to reduce the resistance for the trial velocities. As mentioned earlier, the range of variation of the hull in the forebody is limited, considering restrictions on the cargo capacity and hydrostatic properties, such as the displacement and position of the center of buoyancy. As a consequence, slight modifications are accepted and they are controlled with the definition of design variables and constraints.

Objective Functions:

- Wave resistance coefficient C_w for 13 Kn.
- Wave resistance coefficient C_w for 14 Kn.

Design Variables:

- $-0.3\% \leq \Delta C_P \leq 0.3\%$
- $-0.2\% \leq \Delta C_B \leq 0.2\%$
- $-15^\circ \leq \Delta \alpha_{End_E} \leq 15^\circ$

Constraints:

- $-0.3\% \leq \Delta LCB \leq 0.3\%$
- $-1\% \leq \Delta Displacement \leq 1\%$

In total 433 variations of the model were obtained during the optimization routine. However, the calculation was restricted to models with non active constraints. In total 241 feasible designs were considered and computed for the two objective functions. The convergence history of the valid designs can be seen in **Fig 27**. The wave resistance coefficient values of

the parent design are $C_w = 2.24e - 4$ and $C_w = 2.77e - 4$ for 13 Kn and 14 Kn respectively. The design number 237 was chosen as the optimum design with $C_w = 2.21e - 4$ and $C_w = 2.46e - 4$ for 13 Kn and 14 Kn respectively, with a reduction in the wave resistance coefficient of 6.74% for 13 Kn and 12.36% for 14 Kn, see **Fig 28**.

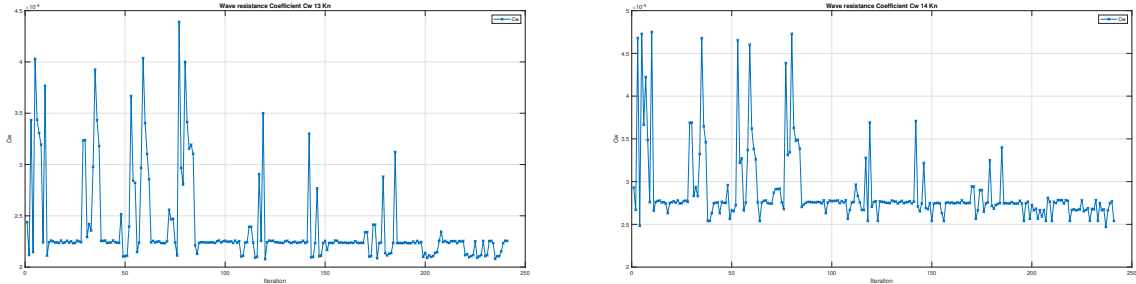


Figure 27: Convergence history plot objective functions

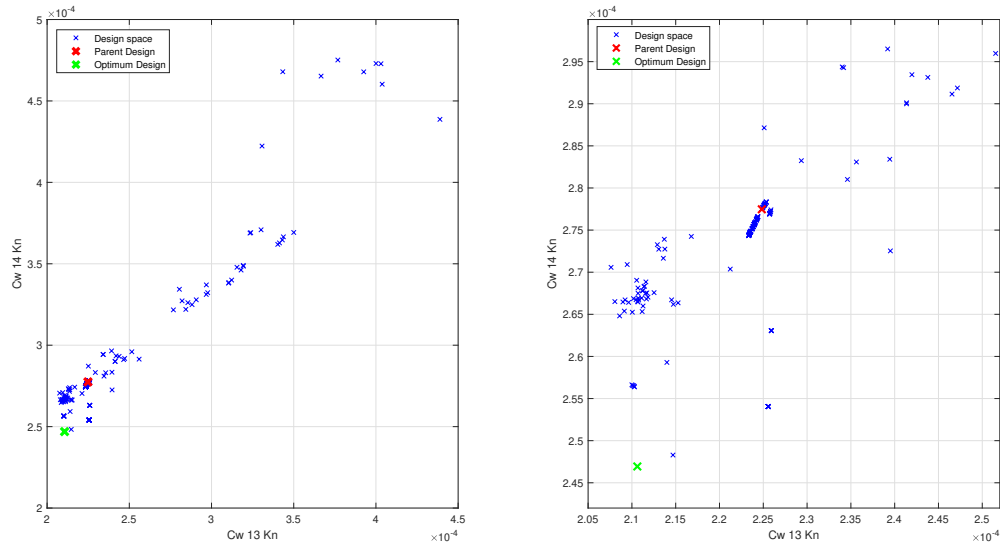


Figure 28: MOGA Comparison

A significant reduction of the wave resistance coefficient was achieved with a slight modification of the hydrostatic characteristics of the ship, satisfying the initial constraints as shown in **Table. 6**.

Table 6: Hydrostatic Properties Variation Fore-body Optimization

	Variation %
C_B	+0.15
C_P	+0.22
Displacement Δ	+0.27
LCB	-0.32

Figure 29 show the variation of the sectional area curve SAC of the fore-body for the parent hull and the optimized hull. It can be seen that the main section was moved slightly forward, thereby increasing the volume on the cargo areas and reducing the volume on the forward section, in which constraints of cargo are not considered.

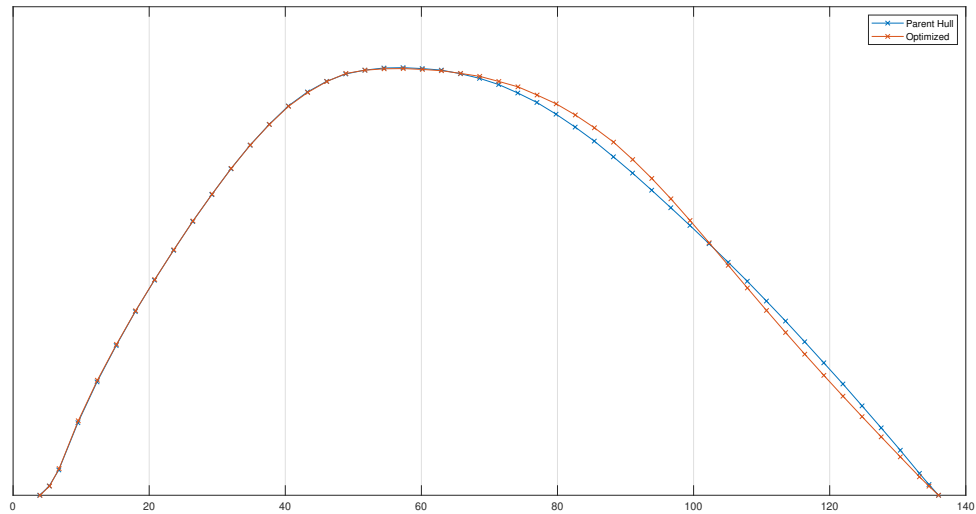


Figure 29: Sectional Area Curve plot

A comparison of the wave pattern of parent and optimized design is plotted for the two objective functions. It can be seen that the wave elevation has been reduced along the length of the optimized hull with a significant variation on the fore-body. Furthermore, the variation of the pressure coefficient between both designs can also be seen in **Fig. 31**.

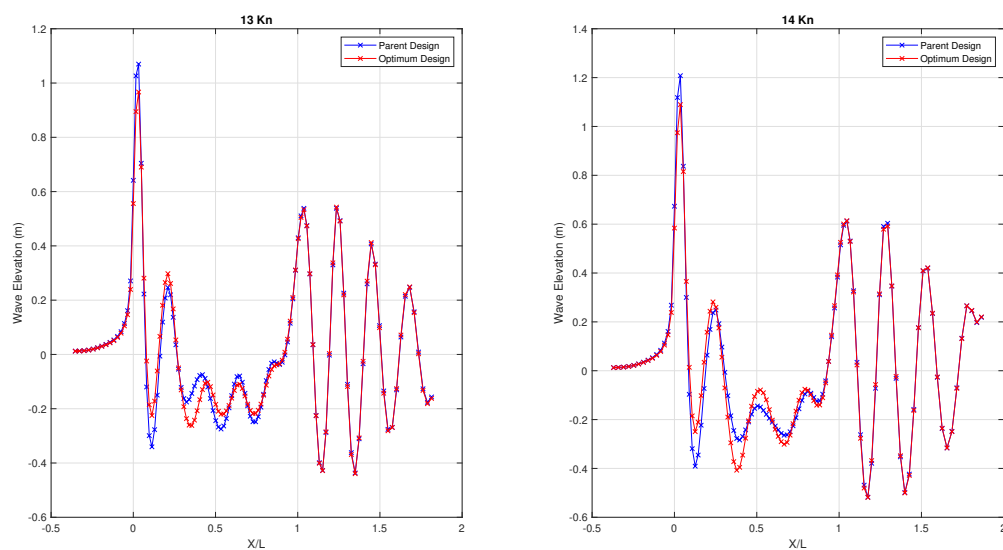


Figure 30: Comparison of the wave profiles of parent and optimized design

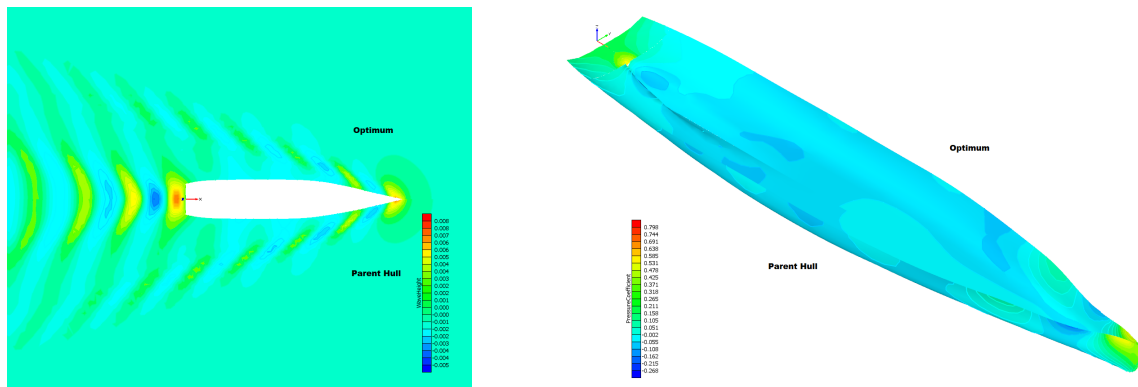


Figure 31: Wave Contour and Pressure coefficient comparison for 13 Kn

5.4 SKEG OPTIMIZATION - ZONAL APPROACH

Based on the hull form obtained from the optimization of the fore-body using *Potential Flow Theory* from **Section 5.3**. The optimization of the skeg using the *Zonal Approach* is performed in this section, considering the effect of the viscosity in the aft-body of the ship and in the wake. The *CPU* time required for a simulation based on a zonal approach was highly increased, compared with the time required for the fore-body optimization. Considering this limitation, a single objective optimization of the total resistance was carried out for a velocity of 14 Kn.

5.4.1 Mesh discretization

The main advantage of the Zonal Approach implemented on Shipflow is the possibility to solve the flow using different methods (see **Fig. 19**), in which the discretization of the domain is reduced. No mesh convergence study was done for this part of the optimization, due to the limitations mentioned earlier. The coarse mesh, automatically done by Shipflow, has an average of 750 000 cells. This coarse mesh was used for each simulation. In **Fig 32**, the viscous domain with the zonal approach can be seen. The free surface is considered as a slip plane that can be fitted with the previous solution of the free surface which is based on *Potential Flow*. A non slip boundary condition is imposed to the aft body and inlet and outlet of the flow were also imposed as can be seen in **Fig 33**.

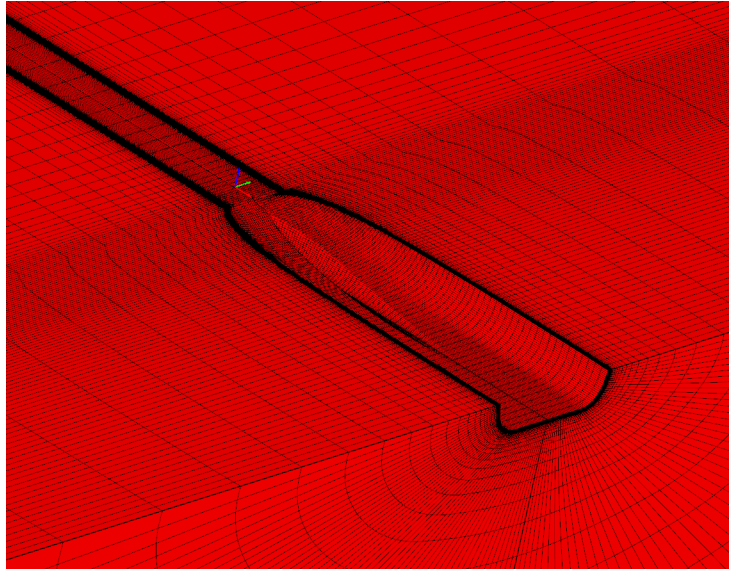


Figure 32: Viscous domain

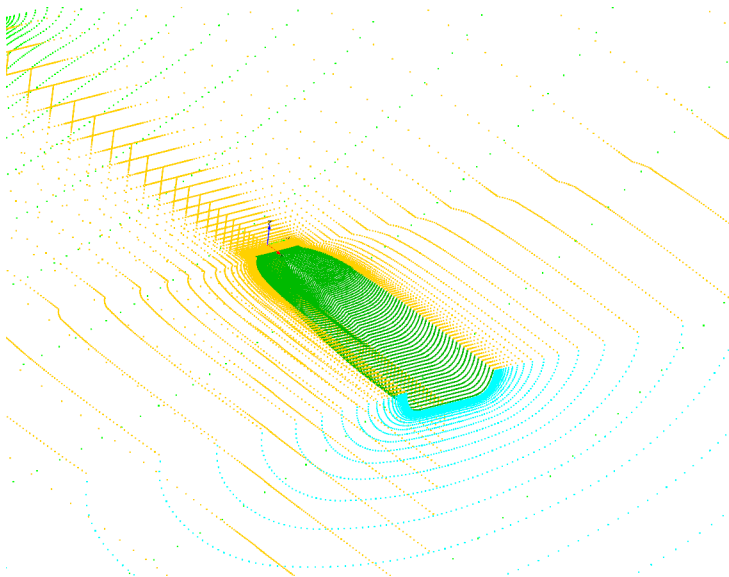


Figure 33: Boundary conditions Zonal Approach

5.4.2 Single Objective Optimization

Considering the increase in the computation time required for the optimization of the aft-body, a different optimization strategy was implemented. In order to analyze the influence of the variables used in the fully parametric approach, an exploration of the design space was carried out using a sampling method "Sensitivity Analysis", which aided to have a better understanding of the design variables influence on the objective function to be optimized.

In total, 27 different designs were simulated with a considerable variation range on 5 different design variables. By using this sampling method, the lower and upper bounds of

every design variable can be restricted in order to use a local optimization method with the reduced design space helping the algorithm to avoid a local minimum, due to the influence on the starting point for these type of methods.

Sensitivity Analysis

Five different parameters previously defined in **Section 5.2.2** were considered as design variables for the fully parametric optimization of the skeg, by defining lower and upper bounds as can be seen in **Table 7** for the exploration of the design space. The definition of the initial bounds was made in order to keep the obtained shape of the skeg found in **Chapter 4**, and to satisfy the minimum distances between the different components of the propulsion system and the hull as defined in **Table 2** which were considered as side constraints for the optimization of the aft-body.

Table 7: Design variables "Sensitivity Analysis"

	Lower bound	Upper bound	Type of Variation
<i>aftTanSkeg</i>	2	25	Differential
<i>skegwidth</i>	0.8	1.2	Integral
<i>Tangentstart</i>	0	10	Differential
<i>xMidSkeg</i>	18	25	Positional
<i>yMaxSkeg</i>	2.4	2.9	Integral

From **Fig. 34**, the influence of each design variable on the objective function can be analyzed to reduce the design space for the next phase of the optimization. It can be seen that the variation of two design variables are of high impact to the objective function. The blue color indicates a trend such that, if the design variable gets increased, the objective function increases as well. The red color indicates a negative correlation; if the design variable gets increased, the objective function decreases. The design variables *aftTanSkeg* and *skegwidth* are considered as important variables and their ranges were modified based on the trend of their correlations.

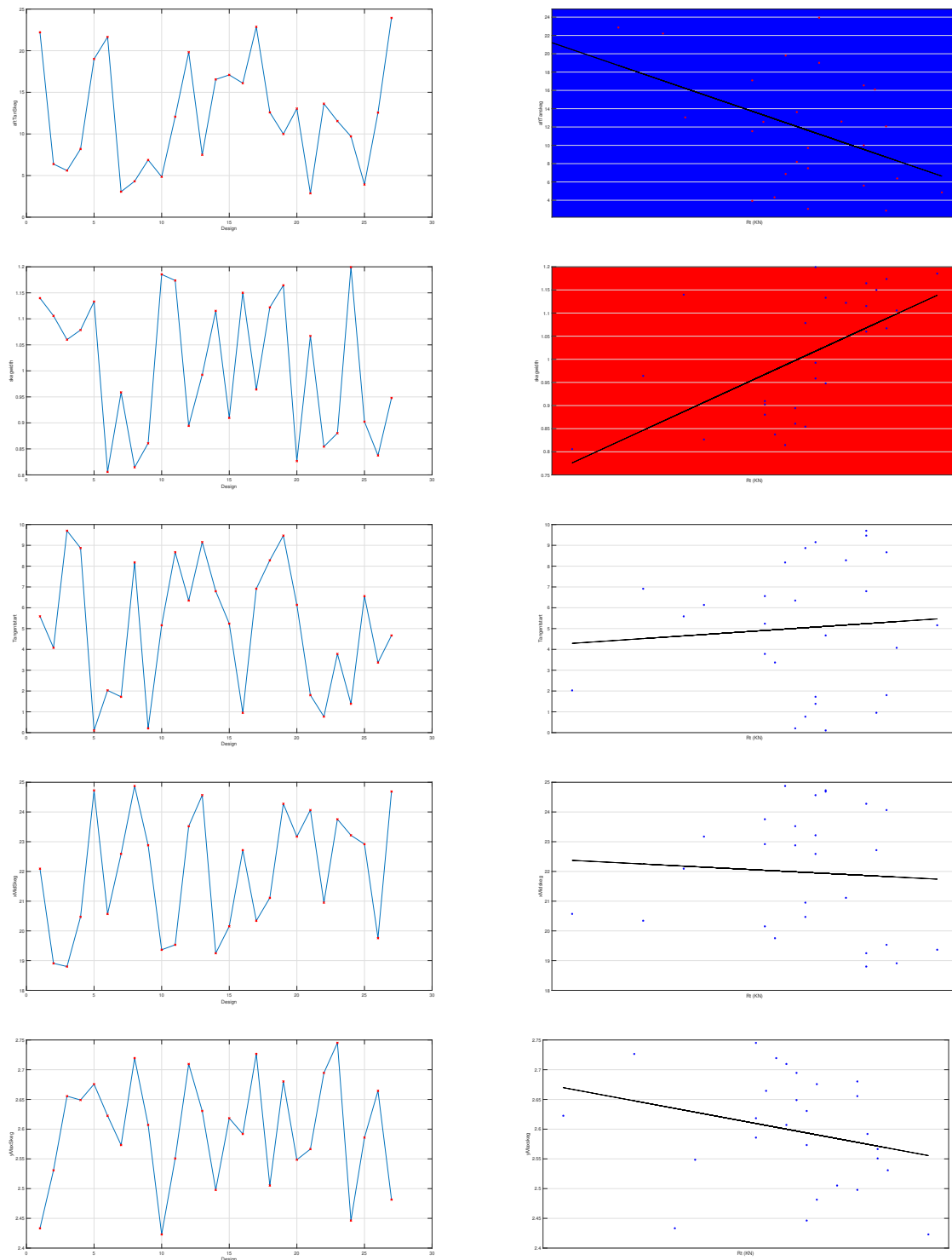


Figure 34: Sensitivity Analysis design Variables

Tangent Search Optimization Algorithm

Local based algorithms are well suited for fast convergence of the objective function, they are being widely used for hull optimization starting from the result of a sampling method in order to avoid local minimum. Based on the results from the sensitivity analysis, this optimization algorithm was used to continue with the skeg optimization. In **Table. 8** the

design variables with the new bounds can be seen.

Table 8: Design variables "T- Search Method"

	Lower bound	Upper bound
aftTanSkeg	22	23
skegwidth	0.8	0.93
Tangentstart	1	5
xMidSkeg	20	22.4
yMaxSkeg	2.4	2.7

Four inequality constraints are considered based on the minimum distances to be kept between the components of the propulsion system and the hull as mentioned before. These constraints are defined with the distance between the projected point from the equipment to the hull and the center line \mathcal{C} .

Inequality Constraints:

- Aft thruster $\geq 0.75m$
- Gearbox $\geq 1.5m$
- Main Engine $\geq 2.1m$
- Displacement $\Delta \geq 10450 \text{ Tons}$

In total, 39 variations of the model were obtained during the optimization routine with the *T-Search method*. From **Fig. 35** the effectiveness of using a sampling method to correctly define the design space before using local based method is observed, thereby making it possible to select a correct starting point, considering that these methods are sensible to the starting points.

After the optimization, a design satisfying all the design constraints is obtained with a reduction of 3.32% of the objective function.

Considering that the optimization of the hull was done using low-fidelity solvers and with coarse mesh using the *Zonal Approach*, the obtained design was validated using high-fidelity solver (*ISIS-CFD*). It is important to note that *Shipflow* is also a high fidelity solver when the flow is fully solved with *RANS* equations. However, for validation purposes, *FineMarine* was used considering that the first *CFD* calculations in which the best shape of hull was defined was done using this solver.

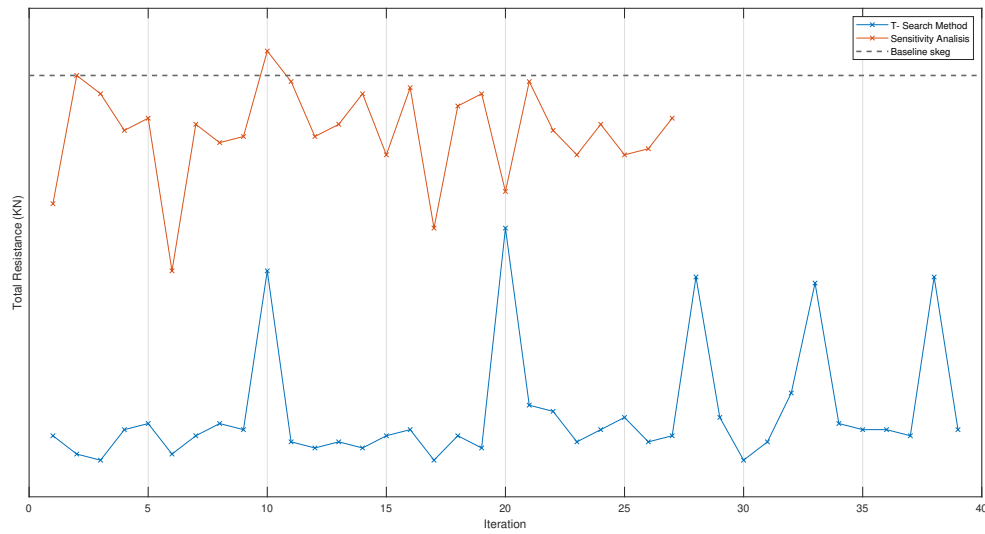


Figure 35: Convergence History Objective Function

The validation of the optimized hull was done using the same parameters stated in **Chapter 4** for all the simulations. In **Table 9**, a comparison between the obtained results for the hull resistance without additional components, efficiency and BHP including additional resistance components required for the optimized velocity can be seen obtaining a considerable reduction with respect to the parent design.

Table 9: Resistance and Powering comparison optimized hull for 14 Kn

	Difference Baseline- Optimized
Hull Resistance (kN)	-2.63
OPC (%)	+1.75
BHP (kW)	-2.59

6 Conclusion and Recommendations

During the course of this work all the objectives were accomplished. Starting with the definition and integration of an Eco-friendly propulsion system following the new regulations regarding the emissions from the ship industry. Different shapes of the hull have been proposed based on this propulsion system, and the performance of each of them for the operating condition of the ship has been studied in detail.

The main goal of this project was to perform a hydrodynamic optimization of the hull which is a relatively new topic for the design industry. Previously, the concept of optimization was far from the application of rigorous optimization methods. In opposition, the optimization term was used when the best design between a set of different models was found, and it was based just on the experience of the Naval Architects and on previous designs. One of the main limitations in the industry is spending a significant amount of resources in terms of computation power. For some special projects in which the resources to perform an optimization are included in the budget, those studies are generally subcontracted to specialized companies with powerful computation clusters and not limited on number of licenses being able to perform multi-objective optimization processes using high fidelity solvers (RANS).

The expected results from a resistance and powering hydrodynamic optimization are sensible to the quality of the starting design, and for new designs this improvement is around 6-8%. The reduction in resistance and powering after this work was around 2.5% which is a satisfactory reduction considering the limitations during the course of this project: on the quality of the discretizations and due to the limited resources in terms of computation power. Also taking into account that the parent hull was considered as a good design.

Reliable results from hybrid optimization strategies have been obtained using both low fidelity and high fidelity solvers during the optimization. These results have been proved at the end with validation using high fidelity solvers.

It is suggested to use this hybrid approach and a rigorous optimization algorithm, instead of running different simulations with high fidelity solvers using trial and error technique during the design process.

References

- [1] D. Hudson A Molland S. Turnock. *Ship Resistance and Propulsion*. Vol. 1. Cambridge University Press, 2011.
 - [2] Bosch A. “Sail Propulsion of Commercial Vessel and Dimensional Tools”. PhD thesis. Hydrodynamics for Ocean Engineering, Ecole Central Nantes, 2019.
 - [3] Flowtech International AB. “XCHAP theoretical manual”. In: (2007).
 - [4] Numeca International AB. “Documentation guide Fine Marine v8.2”. In: (2007).
 - [5] C. Abt and S. Harries. “Hull variation and improvement using the generalized Lackenby method of the FRIENDSHIP SYSTEMS”. In: *The Naval Architect* (2007).
 - [6] Z Long Zhang B. Ji Zhang. *Research on Ship Design and Optimization Based on Simulation-Based Design (SBD) Technique*. ISBN 978-981-10-8422-5. Springer, 2012.
 - [7] V. Bertram. *Practical Ship Hydrodynamics*. Second edition. Elsevier, 2012.
 - [8] J. Carlton. *Marine Propellers and Propulsion*. Vol. Second Edition. Elsevier, 2007.
 - [9] International Towing Tank Conference. “ITTC- Recommended Procedures and Guidelines "Practical Applications for CFD Applications"”. In: (2011).
 - [10] G. Delhommeau. “Wave resistance code REVA”. In: *Numerical Simulation of Hydrodynamics: Ship and Offshore Structures 19 WEGEMT School* (1993).
 - [11] Y. Tahara EF. Campana D. Peri. “Numerical Optimization Methods for ship hydrodynamic design”. In: *Annual meeting* (2009).
 - [12] L. Gentaz. “M2-MTECH-HOE-NUMHY-Navier-Stokes-19-20”. 2020.
 - [13] J. Heimann. “CFD Based Optimization of the Wave-Making Characteristics of Ship Hulls”. PhD thesis. Technical University of Berlin, 2005.
 - [14] R.R. Hilleary. “The Tangent Search Method of Constrained Optimization”. PhD thesis. United States Naval Postgraduate School, 1966.
 - [15] H. Lackenby. “On the systematic geometric variation of ship forms”. In: *Transactions of The Institute of Naval Architects* (1950).
 - [16] L. Larsson. “Resistance and Flow Predictions Using the Shipflow Code”. In: *Numerical Simulation of Hydrodynamics: Ship and Offshore Structures 19 WEGEMT School* (1993).
 - [17] K Susuki M. Masut. “Experimental Verification of Optimized hull form based on Rankine Source Method”. In: (2001).
 - [18] F.R. Menter. “Zonal Two Equation $k-\omega$ Turbulence Models for Aerodynamic Flows”. In: *24th Fluid Dynamics Conference* (1993).
 - [19] JH. Michell. *The Wave Resistance of a Ship*. 45th ed. Philosophical Magazine, 1898.
-

-
- [20] International Maritime Organization. *Nitrogen Oxides NO_x- Regulation 13*. URL: [http://www.imo.org/en/OurWork/Environment/PollutionPrevention/AirPollution/Pages/Nitrogen-oxides-\(NOx\)-%E2%80%93-Regulation-13.aspx](http://www.imo.org/en/OurWork/Environment/PollutionPrevention/AirPollution/Pages/Nitrogen-oxides-(NOx)-%E2%80%93-Regulation-13.aspx) (visited on 08/10/2020).
- [21] A. Papanikolaou. *A Holistic Approach to Ship Design*. Vol. 1. Springer.
- [22] Harries S. “Parametric Design and Hydrodynamic Optymization of Ship Hull Forms”. PhD thesis. Technical University of Berlin, 1998.
- [23] J. Wakers. “Adaptive Grid Refinement for Hydrodynamics Flow Simulation”. In: *An International Journal Computer and Fluids* 55 (2012).
-